Journal of Marine Systems 187 (2018) 260–276

Contents lists available at ScienceDirect

Journal of Marine Systems

journal homepage: www.elsevier.com/locate/jmarsys

A large-scale view of oceanic variability from 2007 to 2015 in the global high resolution monitoring and forecasting system at Mercator Océan

Florent Gasparin[a,*], Eric Greiner[b], Jean-Michel Lellouche[a], Olivier Legalloudec[a], Gilles Garric[a], Yann Drillet[a], Romain Bourdallé-Badie[a], Pierre-Yves Le Traon[a,c], Elisabeth Rémy[a], Marie Drévillon[a]

[a] Mercator-Ocean International, 10 Rue Hermès, Ramonville-Saint-Agne 31520, France
[b] CLS, 11 Rue Hermès, 31520 Ramonville-St-Agne, France
[c] Ifremer, 29280 Plouzané, France

ARTICLE INFO

Keywords:
Global ocean monitoring and forecasting system
Climate variability
System evaluation/qualification
Global ocean observing system

ABSTRACT

The global high resolution monitoring and forecasting system PSY4 at Mercator Océan, initialized in October 2006, has achieved 11 years of global ocean state estimation. Based on the NEMO global 1/12° configuration, PSY4 includes data assimilation of satellite and multi-instrument *in situ* observations. In parallel to this monitoring system, a twin-free simulation (with no assimilation) has been performed for the period 2007–2015. In this study, monthly-averaged fields of both ocean state estimates are compared with observation products for the period 2007–2015, to examine the consistency of PSY4 fields with related observations for representing large-scale variability and to provide a baseline that is mainly focused on *in situ* comparisons for validation/qualification of on-going system developments. Observations play a major role in correctly positioning the main energetic structures, both in space and time. In addition, data assimilation appears to overcome the other deficiencies of models by reducing SST bias in upwelling regions and by increasing the thermocline gradient in the tropics. Generally, the amplitude of the total-resolved variability in both PSY4 estimates is consistent with observation data sets. Annual cycle and longer-term variability in temperature, salinity and sea surface height are significantly improved with data assimilation, but some progress is still needed to better represent the amplitude of changes of ocean heat and freshwater contents on long timescales. Finally, the PSY4 system's ability to capture the large scale variability is further investigated by using as a case study the northward pathways of El Niño anomalies in the tropical North Pacific in 2014 and 2015 in order to illustrate how such systems can be used to answer relevant scientific questions.

1. Introduction

Observing and modeling the global ocean are crucial for describing and predicting basin-wide oceanic variability, in addition to local phenomena, and regional to global scales. During the last two decades, the development of new technologies, including advanced satellite and *in situ* instruments, combined with significant progress in modeling and data assimilation techniques, have revolutionized oceanography (Le Traon, 2013). These scientific advances have converged in an integrative approach through operational oceanography, which benefits society through related downstream services (She et al., 2016). Progress in operational oceanography has mainly been accomplished through advanced ocean modeling and data assimilation science and technology, carried out in the framework of the Global Ocean Data Assimilation Experiment (GODAE) Ocean View (Bell et al., 2015). In the meantime, the ability of operational ocean monitoring and forecasting systems to monitor the global ocean in four dimensions has been significantly improved by complementary information from satellite and *in-situ* observations, which are part of the integrated Global Ocean Observing System (Legler et al., 2015).

The present work is based on the global ocean system at 1/12° horizontal resolution developed at Mercator Océan, PSY4V3R1, which has been implemented as the global high resolution physical monitoring and forecasting system, operated in near real time by the Copernicus Marine Environment Monitoring Service (CMEMS) since 19 October 2016. The recent technical updates of modeling schemes and estimation tools applied to this system are detailed in a related paper by Lellouche et al. (2018), which gives an assessment of their impact on

* Corresponding author.
E-mail address: fgasparin@mercator-ocean.fr (F. Gasparin).

https://doi.org/10.1016/j.jmarsys.2018.06.015
Received 17 January 2018; Received in revised form 25 June 2018; Accepted 26 June 2018
Available online 30 June 2018

the product quality as compared to its previous version, using the usual qualification/validation metrics for operational systems. In order to assess the stability over time, data assimilation performance and error setting, this system has been initialized on 11 October 2006, providing a long period of ocean analysis fields ("hindcasts"). As this 10-yr time series benefits from reprocessed and delayed-time data, it can be seen as a "short reanalysis ", which allows more robust statistical analyses in comparison to the previous versions (e.g., Lellouche et al., 2013). In this study, we focus on the 2007–2015 period, the near real time ocean estimates (i.e., the post October 2016 period) are thus not considered. In addition, the study focuses on the open ocean in the latitude band between 65° S and 65° N, because the complexity of polar regions, including the presence of continental and floating ice, requires specific validation/qualification procedures (e.g., Koenig et al., 2017).

A primary objective of this work is to demonstrate the scientific value of the Mercator Océan monitoring and forecasting system for resolving oceanic variability at regional and global scales, and to provide key characteristics and validation metrics for further scientific use. By comparing it with a twin-free simulation, in which no satellite or *in situ* data are assimilated, another objective is to quantify the "skill assessment", i.e, how global ocean observations improve the representation of the large-scale ocean state, but also to determine what is missing in the free simulation. These improvements aim at demonstrating the critical need to sustain and enhance *in situ* and remote-sensing measurements in order to improve the proficiency of monitoring and forecasting systems. Furthermore, assessing the ability of the twin-free simulation to represent the large-scale mean and variability is of interest for several fields of scientific research focusing on physical and/or biological mechanisms (e.g., Raghukumar et al., 2015), but also in the context of observing system simulation experiments (OSSE), such as performed in the framework of the European Horizon 2020 AtlantOS project (Visbeck et al., 2015, https://www.atlantos-h2020.eu) or coupled climate models (Reichler and Kim, 2008).

It is noteworthy that monitoring and forecasting systems assimilate almost all of the information from satellites and multi-instrument *in situ* databases (e.g., from CORIOLIS, Cabanes et al., 2013), making comparison with independent observations difficult. The evaluation/qualification procedures of model fields integrate a range of complementary metrics (Crosnier and Le Provost, 2007; Hernandez et al., 2015). These include for instance eyeball verification of synoptic structures against satellite observations, mean and root-mean-square deviations from satellite and *in situ* observations, plus consistency checks of integrated quantities (e.g., heat and freshwater contents, transports) with respect to reference values deduced from observations. For instance the ocean forecasting systems comparison exercise described in Ryan et al. (2015) is based on departures from observations averaged in the observation space, which makes it possible to evaluate how operational systems have ingested available information to fit observations. Note that the integrated feature of an operational system, combining satellites and *in situ* observations associated with the underlying model dynamics and assimilation procedures, does not guarantee that all information is retained.

Metrics designed to assess long-term variability are therefore usually applied to reanalyses which span at least 10 years (Balmaseda et al., 2015), while real-time forecasting systems, usually restricted to a couple of years, focus on the accuracy of high frequency variability evaluated from a 1 or 2-yr time series. The near-real time protocol adopted by Mercator Océan then consists in a 10-yr time series of hindcasts before entering into operation. This complete PSY4 fields are thus compared with interpolated observation data sets in order to assess the PSY4 system's ability to represent the 2007–2015 mean, annual cycle, and longer-term variability at a near-global scale. The analysis may therefore depend on interpolation procedures from observation data sets, but the objective is to put monitoring and forecasting system fields on the same level as standard data sets commonly used in the oceanographic community.

The paper is organized as follows. Section 2 presents the PSY4V3R1 model and data assimilation system, as well as the observation products used for comparison to the monitoring and forecasting system. The upper-ocean mean is described in Section 3. InSection 4, the 2007–2015 oceanic variability embedded in the monitoring and forecasting system fields, including annual and longer-term variability, is detailed. In addition, the case study of the El Niño anomalies in the tropical North Pacific in 2014/2015 illustrates how such systems can be used to answer relevant scientific questions. The conclusions are given in Section 5.

2. The Mercator Océan system and observation data sets

2.1. The Mercator Océan monitoring and forecasting system PSY4V3R1

The global high resolution monitoring and forecasting system PSY4V3R1 (hereafter referred to as PSY4) is based on version 3.1 of the NEMO ocean model (Madec and the NEMO team, 2008), which uses a 1/12° ORCA grid type (with a horizontal resolution of 9 km at the equator, 7 km at mid-latitudes and 2 km near the poles). The water column is discretisized into 50 vertical levels, including 22 levels within the upper 100 m, with 1-m resolution at the surface and 450 m resolution at the bottom. The bathymetry is a combination of interpolated ETOPO1 (Amante and Eakins, 2009) and GEBCO8 (Becker et al., 2009) databases. The PSY4 system was initialized on 11 October 2006, based on the temperature and salinity profiles from the EN4 monthly gridded climatology (Good et al., 2013), averaged for the period October–December 2006. Assuming that the velocity field is zero at the start, the model physics then spins up a velocity field in balance with the density field. More details about the spin-up procedures can be found in Lellouche et al. (2018). The atmospheric fields, which force the ocean model, are obtained from the European Centre for Medium-Range Weather Forecasts-Integrated Forecast System (ECMWF-IFS) at 3-hr resolution, in order to reproduce the diurnal cycle. A mean dynamic topography (MDT), based on the "CNES-CLS13" MDT and taking into account the EGM-DIR R4 model of the GOCE geoid, has been used (Rio et al., 2014). More details concerning parameterization of the terms included in the momentum, heat and freshwater balances (i.e, advection, diffusion, mixing or surface flux) or MDT procedures can be found in Lellouche et al. (2018).

Satellite altimetry, sea surface temperature (SST) and sea ice concentration observations, operationally produced by CMEMS (http://marine.copernicus.eu/), are assimilated in the system. This consists of along-track sea level anomaly data from the Data Unification and Altimeter Combination System (DUACS) multi-mission altimeter products and gridded OSTIA SST (*Operational sea surface temperature and sea ice analysis*), which combines satellite SST data (*Group for High Resolution Sea Surface Temperature* project, GHRSST) with *in-situ* observations (Donlon et al., 2012). Additionally, satellite sea ice concentration from the EUMETSAT/Ocean and Sea Ice Satellite Application Facility (OSI SAF) is now assimilated in the PSY4 system (No ice assimilation in Lellouche et al., 2013). Subsurface vertical profiles of temperature and salinity from the CORA 4.1 *in situ* database (Cabanes et al., 2013; Szekely et al., 2016) have been assimilated for the period considered in the paper (2007–2015). This database includes vertical temperature and salinity profiles from Argo floats, moorings, gliders, expendable bathythermograph (XBT) transects, sea mammals, and conductivity-temperature-depth (CTD) casts from oceanographic cruises. Low-quality profiles were excluded after several quality control tests were performed as described in Lellouche et al. (2018). In Fig. 1, the number of temperature profiles with data to 1000 m or deeper, which have been assimilated in the monitoring and forecasting system, are shown for the year 2007 (a total of 76,216 profiles) and the year 2015 (a total of 126,282 profiles). The quite heterogeneous distribution in space and time of the *in situ* observing system mostly reflects the development of the Argo array since 2000s, whose coverage is best for

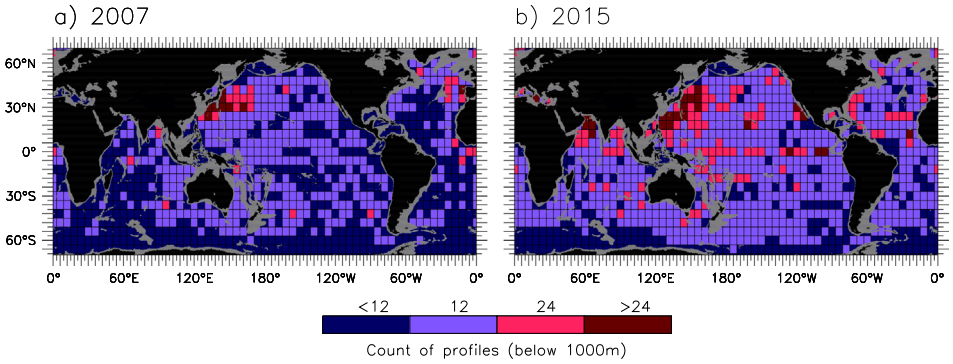

Fig. 1. 6° × 6° binned count of temperature profiles (CTD, glider, Argo, mooring, XBT, sea mammals) per month with data to 1000 m or deeper for the years (a) 2007 and (b) 2015. Note that the number of 12 profiles per 6° × 6° bin per month is equivalent to 1 float per 3° × 3° bin (initial Argo design).

the Kuroshio Extension region (Roemmich and Gilson, 2009).

These satellite and *in situ* observations are assimilated using a reduced-order Kalman filter derived from a SEEK filter (SAM2, Brasseur and Verron, 2006). An adaptive tuning of observation errors for altimetry and SST has been implemented in order to refine the prescription of observation errors (Desroziers et al., 2005). There is no SST/SSS relaxation in either of the two simulations. A weak constraint with respect to the World Ocean Atlas 2013 (2005–2012) climatology on temperature and salinity in the deep ocean (below 2000 m) has been included to prevent large deviations from climatology. The method consists in assimilating virtual vertical climatological profiles of temperature and salinity below 2000 m, using a density criterion (departure from climatology) depending on latitude and depth, as detailed in Lellouche et al. (2018). Concretely, this procedure is applied to some regions where the steep bathymetry might be an issue for the model (i.e., Kerguelen Plateau, Zapiola Ridge, and Atlantic ridge) and mostly concerns western boundary current (WBC) regions of the North and South Atlantic and along the Antarctic Circumpolar Current (ACC). More details can be found in Lellouche et al. (2018, see their Figs.10 and 11). Note that this procedure is not applied in the twin-free simulation. In addition, a 3D-Var correction for the slowly evolving large-scale error of the model in temperature and salinity is applied (Lellouche et al., 2013). More details on the data assimilation procedures can be found in Lellouche et al. (2013) and Lellouche et al. (2018).

The global high resolution ocean monitoring and forecasting system PSY4 provides daily monitoring and forecasting outputs. Monthly-averaged analysis fields were used in this study. A twin simulation ending in 2015, in which no satellite or *in situ* data were assimilated, was performed in parallel to the monitoring and forecasting system using the same initialization. To distinguish between them, fields from the monitoring and forecasting system are called 'PSY4 Oper', and fields from the free simulation 'PSY4 Free'. The analysis was performed for the 9-yr common period 2007–2015. The monthly PSY4 fields of potential temperature, salinity, and sea surface height were obtained by using monthly-averaged fields for each month over the 9-yr period.

2.2. The SCRIPPS Argo and the DUACS satellite altimetry products

The SCRIPPS Argo and DUACS satellite altimetry products were used to assess PSY4's ability to represent large-scale quantities. As mentioned previously, these data products are not independent of the PSY4 Oper solution, but are products based on a single instrument type and use their own interpolation techniques. Gridded monthly *in situ* temperature and salinity fields have been provided by the SCRIPPS Argo climatology since 2004 for the global ocean (Roemmich and Gilson, 2009), and have been downloaded from the dedicated SCRIPPS Argo website (http://www.argo.ucsd.edu/). This 1° × 1° horizontal resolution product has 58 pressure levels from the surface to 2000 dbar, with separate levels spaced from 10 to 100 dbar in the deeper ocean. Satellite altimeters provide SSH anomaly estimates, from the DUACS delayed-mode merged product from October 1992 to December 2015. This consists of gridded SSH anomalies combining all available satellite altimeters. The 2014 DUACS product with a 1/4 ° × 1/4° horizontal resolution provides monthly-averaged maps, and has been downloaded from the CMEMS catalogue (http://marine.copernicus.eu/). Anomalies from the 2007 to 2015 annual mean have been considered.

3. The 2007–2015 annual mean

Monthly PSY4 temperature and salinity fields were used to calculate potential density and steric height (SH). For zonally and globally averaged quantities, latitudes higher than 65° have been masked out. The comparisons to the SCRIPPS Argo product are limited to the mask of the SCRIPPS Argo product, in which marginal seas and the Arctic Ocean are excluded. In order to compare PSY4 fields with gridded standard products, the PSY4 fields were moved from the irregular NEMO grid to the 1° × 1° regular grid of the SCRIPPS Argo product and the 1/4 ° × 1/4° regular grid of the DUACS product, using a bilinear 2D interpolation (SOSIE software, see Brodeau, 2007).

3.1. Sea surface temperature and sea surface salinity

In Fig. 2a, b, the 9-yr mean of temperature and salinity at 5 m depth, which are considered as SST and SSS, is shown with contours for SST from the PSY4 means (PSY4 Oper and PSY4 Free) and color shading for "PSY4 minus Argo" SST differences (i.e., Oper-minus-Argo, Free-minus-Argo). Because the Argo CTD pump is conventionally cutoff to 5 dbar as the float rises to the surface to avoid possible contamination in the conductivity cell (Riser et al., 2008), the comparison is thus done at the depth of 5 m. Note that PSY4 Oper and Argo fields are not independent since Argo profiles are assimilated in PSY4 Oper. Compared with SST, PSY4 sea surface salinity (SSS) is not directly constrained by satellite SSS, but SSS satellite measurements suffer from large biases of up to several hundreds of kilometers from coastlines (Boutin et al., 2013). The comparison of PSY4 fields with satellite SSS would thus hardly be conclusive, consequently PSY4 SSS is also evaluated by using the SCRIPPS Argo product (Fig. 2c, d).

In Fig. 2b, Free-minus-Argo SST differences show distinctive patterns. A large zonal band of negative anomalies is located south of 20° S, with values exceeding −1.5°C along the Subantarctic front south of Africa. The tropical band is marked by positive anomalies at the eastern boundaries of the basins (up to 1.5°C in the Gulf of Guinea) and Indonesian seas. In addition, regions with a strong SST meridional gradient, such as in the Gulf Stream and Kuroshio regions, have strong biases, with the pattern of a dipole (positive anomaly at the north, and negative anomaly at the south). These large-scale differences reflect complex research issues in ocean general circulation models for

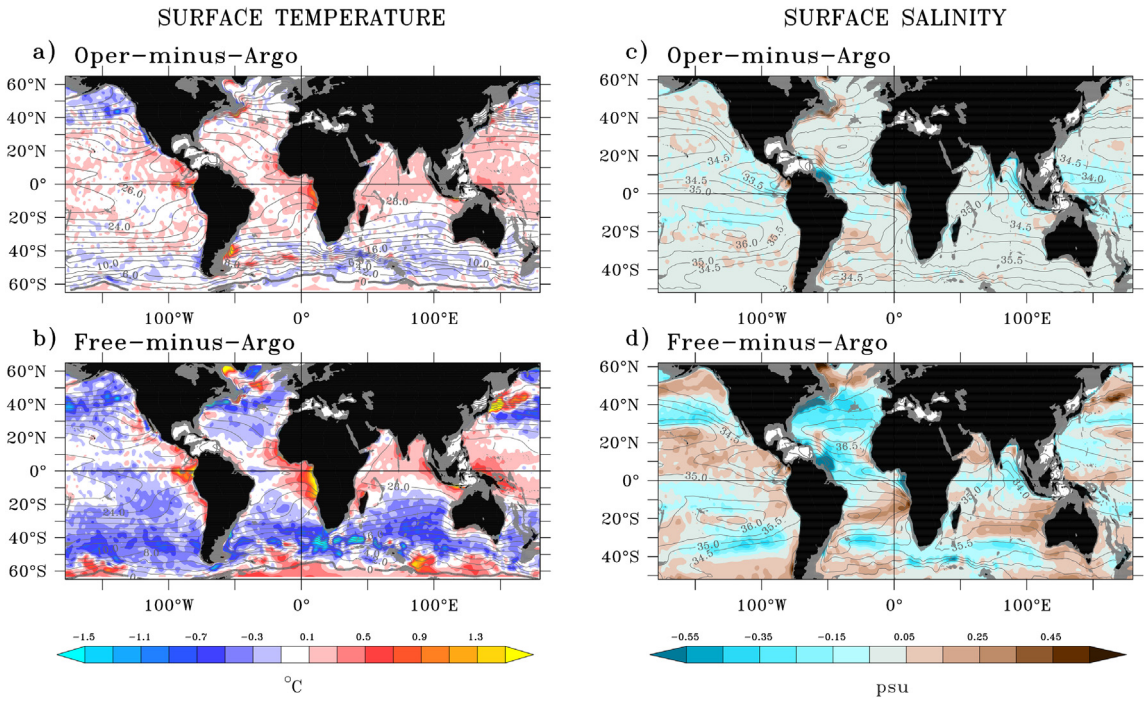

Fig. 2. (a) SST annual means from PSY4 Oper (contours) and Oper-minus-Argo difference (color shading). Gray shading indicates bathymetry shallower than 2000 m depth. PSY4 and Argo fields are considered for the period 2007–2015. Unit is °C. (b) Same except from PSY4 Free. (c, d) Same as (a, b), except for SSS. Unit is psu. (For interpretation of the references to color in this figure legend, the reader is referred to the web version of this article.)

modeling SST fronts, WBC regions, and surface cooling processes in upwelling regions, including vertical mixing, air-sea coupling and ocean advective mechanisms (e.g., Kelly et al., 2010; Toniazzo and Woolnough, 2014).

In order to improve SST representation from PSY4, assimilation of *in situ* and satellite data can constrain model estimates in favor of observations, which significantly reduces Oper-minus-Argo differences such as in the Subantarctic front (Fig. 2b). However, small positive anomalies of the order of 0(0.1°C), i.e., PSY4 Oper SST is higher than the SST from the Argo product, persist in the tropical band. The comparison of PSY4 Oper with satellite NOAA OI SST (Reynolds et al., 2002) shows that the main PSY4 Oper minus NOAA SST differences are around than 0.1 °, except in complex coastal upwelling regions having similar warm bias to that in Fig. 2a. Globally, the spatial RMS of the mean difference between PSY4 and Argo SST is 0.31°C for PSY4 Free, and only 0.17°C for PSY4 Oper, with a stronger improvement in the Southern Ocean than in the tropics.

In Fig. 3, the near-surface horizontal circulation at 15 m shows that WBCs are stuck to the coast in PSY4 Free as opposed to the drifter-derived monthly climatology produced by NOAA (Laurindo et al., 2017, downloaded from the website http://www.aoml.noaa.gov/phod/dac). In addition, Free-minus-Argo SST differences are plotted versus latitude in the WBC regions and demonstrate that the SST meridional gradient of PSY4 Free is too strong as compared with that of Argo, and the drifter-derived climatology. In PSY4 Oper, the position of the WBCs and the meridional SST gradient are consistent with the drifter-derived climatology. This supports that data assimilation strongly increases the representation of frontal regions by improving the position of the WBCs.

Compared with the SCRIPPS Argo product, the mean SSS fields of PSY4 Free reveal large-scale biases of around 0.2 psu (Fig. 2d) all over the globe. Those are mainly located at the southern and northern boundaries of the subtropical gyres, indicating that PSY4 Free hardly represents the amplitude and extension of tropical and subtropical gyres. In general, the extension of the gyres is weaker in PSY4 Free than Argo. It has been recognized for a long time that mean surface salinity patterns reflect the overlying patterns of evaporation and precipitation to the first order (Wust, 1936). Uncertainties about the global water cycle can thus directly impact freshwater forcing, including atmospheric and continental components (Yin et al., 2004; Tian et al., 2009; Stephens et al., 2010). In addition, significant anomalies are also found along the coast of the western tropical Atlantic and mostly reflect the complex representation of SSS in the discharge of the Amazon and Orinoco rivers (Labat et al., 2005). The assimilation of observations significantly reduces these large-scale differences to around 0.05 psu (Fig. 2d). However, some remaining discrepancies appear in the Amazon and Orinoco discharge regions, where large water volumes affect the hydrological cycle and the ocean thermodynamic (e.g., Foltz and McPhaden, 2009). The representation of SSS should be further improved with the assimilation of qualified satellite SSS observations (Vinogradova et al., 2014) and better runoff prescription in the future.

3.2. Upper-ocean stratification

Figs. 4 and 6 show similar comparisons to that in Fig. 2, but in the subsurface ocean, at depths of 100 m and 1000 m. As for SST, PSY4 Free-minus-Argo temperature differences are great in strong meridional gradients at mid-latitudes, such as in WBC regions. However, the most prominent pattern is found in the tropical band, where temperature differences are significantly strong (> 2.5°C). A large "horseshoe pattern" appears especially in the Atlantic and Pacific, with zonally elongated positive anomalies in the equatorial eastern basin, and negative anomalies in off-equatorial regions. These anomalies are significantly reduced with data assimilation, even though positive anomalies are still observed in the tropical Pacific and Atlantic.

Fig. 5a, b shows a vertical section of Oper-minus-Argo temperature differences above 300 m along the equatorial Pacific. At the thermocline depth, a positive anomaly in the eastern Pacific can be associated with a deeper thermocline in PSY4 Oper (~20 m) than in Argo, and vice versa in the far western Pacific, suggesting that the zonal tilt of the thermocline is too weak in PSY4 Oper and PSY4 Free. However, negative anomalies are generally found above the thermocline, while

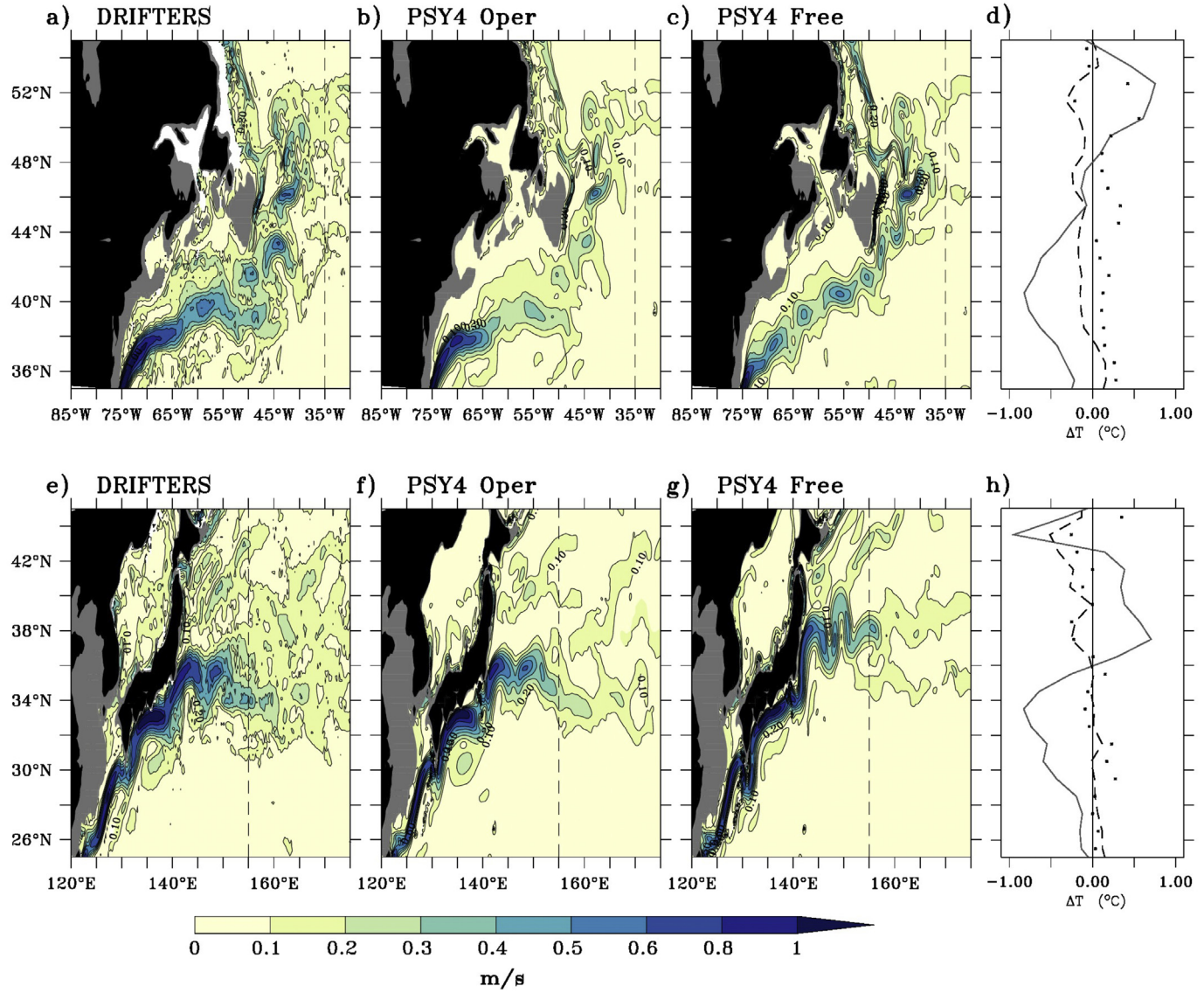

Fig. 3. (a–c) Annual mean of the current velocity at 15 m in the Gulf Stream region from (a) the drifter-derived climatology produced by NOAA, (b) PSY4 Oper and (c) PSY4 Free. In (d), SST differences with the SCRIPPS Argo product for PSY4 Free (gray line), PSY4 Oper (dashed line), and the drifter-derived climatology (dotted line) at 35° W. (e–h) Same as (a–d), except in the Kuroshio region. In (h), SST differences are shown at 155° E. Note that the horizontal velocity is not directly constrained in the PSY4 system. Unit is in m/s for current velocity.

positive anomalies lie below the thermocline. This pattern is even stronger in Free-minus-Argo differences. In Fig. 5c, the mean profiles of PSY4 Oper and PSY4 Free are compared with that of Argo in the eastern Pacific (at 125° W, 0°), revealing strong depth gradient discrepancies between PSY4 Free and Argo (PSY4 Oper is much closer to Argo). This demonstrates that observed patterns in Fig. 4a, b are mostly due to the depth gradient along the thermocline, which is too weak in both PSY4 fields in comparison to observations. Several reasons, including advection errors, may explain the observed differences. In non-advective regions (e.g., at the center of the gyres), errors can be due to uncertainties associated with vertical mixing and atmospheric forcing. In Fig. 6, "PSY4 minus Argo" salinity differences are shown at 100 m and 1000 m depth. Generally, salinity patterns at 100 m are similar to that at the surface (Fig. 2a, b), suggesting that the hydrological cycle affects the upper-ocean down to 100 m. The Free-minus-Argo differences are of the order of 0(0.1 –0.2), while Oper-minus-Argo differences are generally lower than ± 0.05 psu. This demonstrates a clear improvement of the salinity patterns in PSY4 Oper fields.

At 1000 m, the mean temperature from PSY4 Free fields is marked by a global negative anomaly (−0.1°C), and a strong dipole in the northern Atlantic, with a negative anomaly in the west of the basin and a positive anomaly in the east. This dipole disappears in the PSY4 Oper fields. An examination of isotherms at a depth of 1000 m reveals that assimilation induces an upward deflection of isotherms in the west and a downward deflection in the east (~100 m), suggesting that the zonal tilt of the North Atlantic subtropical gyre is too strong in the PSY4 Free fields, and corrected in PSY4 Oper in agreement with Argo. Similar salinity patterns to that of the 1000-m temperature are seen in the North Atlantic in Fig. 6c, d, thus confirming the corrected tilt of the North Atlantic subtropical gyre delimited by density surfaces in PSY4 Oper.

3.3. Steric height and mean circulation

In order to investigate the representation of the subtropical gyres in PSY4 fields, Fig. 7a, b shows contours of the mean SH of the sea surface relative to 2000 m (0/2000 SH) from both PSY4 fields, and color shading indicating the Free-minus-Argo and Oper-minus-Argo 0/

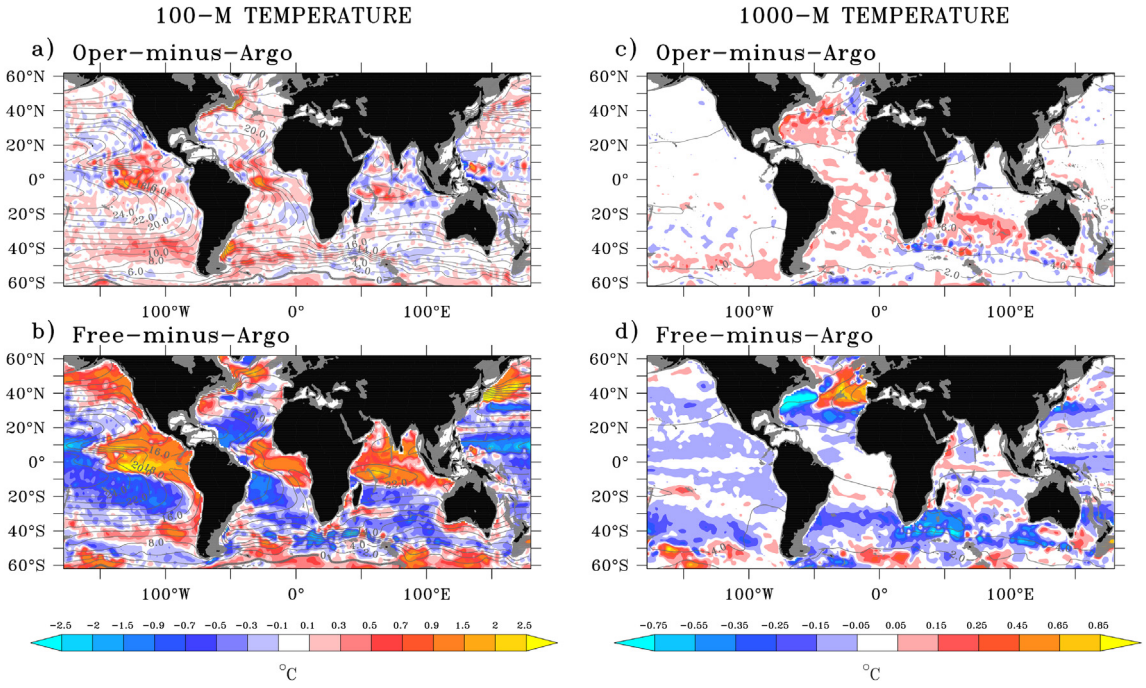

Fig. 4. Same as Fig. 2, except for temperature at 100 m and 1000 m.

2000 SH differences. The five subtropical gyres are evident, with the North Pacific subtropical gyre as the strongest of the five (> 270dyn cm). As previously mentioned for SST, strong Free-minus-Argo 0/2000 SH differences were found in the Southern Ocean and at the western boundaries. Those are related to the position of the main energetic structures, i.e, the Gulf Stream, Kuroshio and Antarctic Circumpolar Current (ACC). Generally, data assimilation significantly reduces Oper-minus-Argo 0/2000 SH differences (Fig. 7b). However, strong positive anomalies persist in the Atlantic WBC regions. These coastal energetic regions, in which high eddy activity drives a lower signal-to-noise ratio, might not be sufficiently sampled by Argo thus leading to relatively high Oper-minus-Argo differences (Fig. 1).

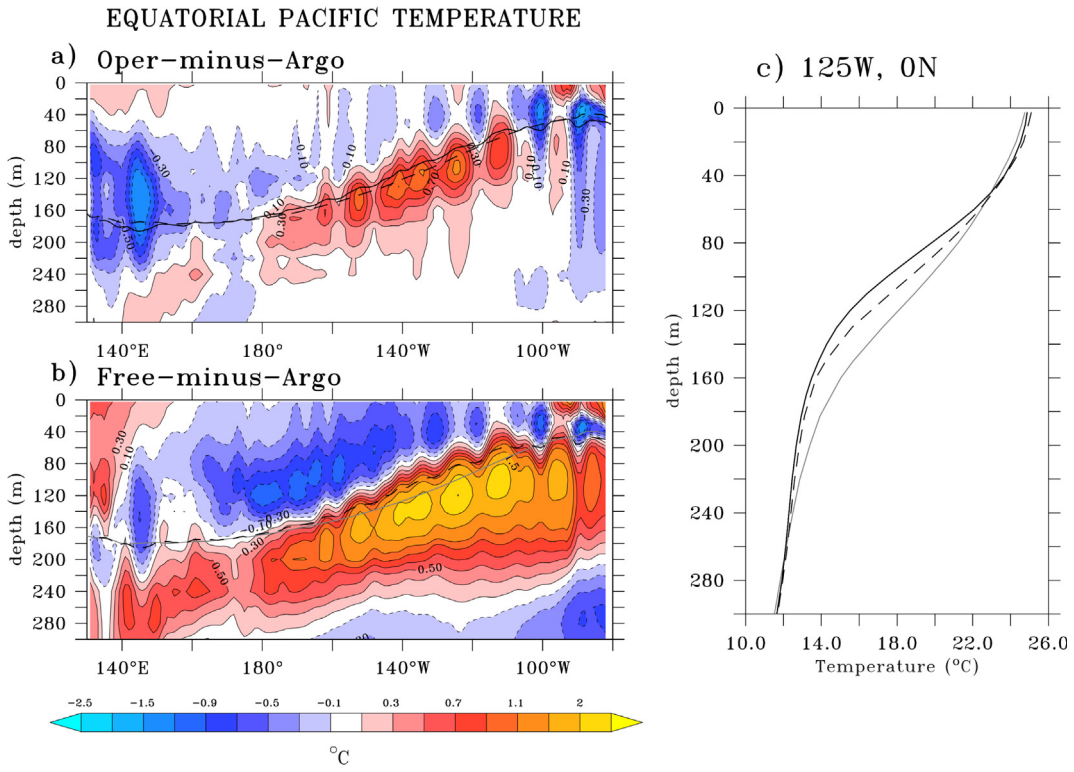

Fig. 5. (a) Mean temperature Oper-minus-Argo difference above 300 m in the equatorial Pacific. The solid black line indicates the PSY4 Oper pycnocline depth (σ = 1025 kg/m^{-3}), and the dashed line indicates the Argo pycnocline depth. (b) Same except for PSY4 Free. (c) Mean temperature profile in the central-eastern Pacific (125° W, 0° N), for Argo (solid black), PSY4 Oper (dashed black), PSY4 Free (gray). Argo, PSY4 Oper and PSY4 Free are considered for the period 2007–2015. Unit is in °C.

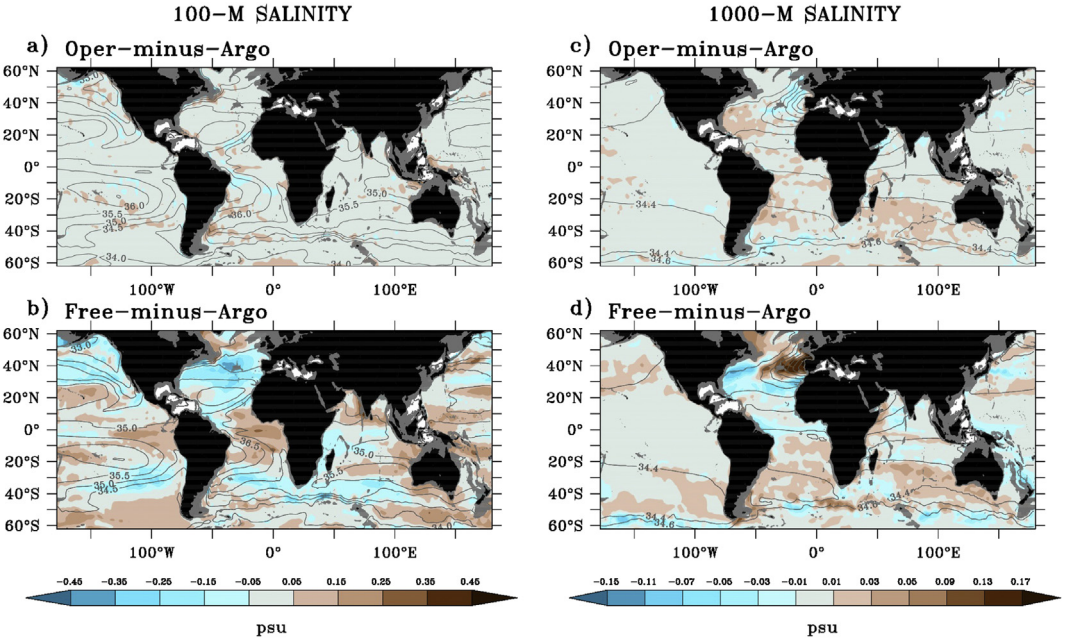

Fig. 6. Same as Fig. 2, except for salinity at 100 m and 1000 m.

Conversely, the Kuroshio region, which is seen as a pilot region for Argo enhancement in the WBCs, does not show such large differences. Other basin scale anomaly patterns (for instance the positive anomaly in the Atlantic Ocean) would require further investigations.

At a deeper level, the 1000/2000 m SH (1000/2000 SH) shows the high amplitude of the Southern Hemisphere gyres in comparison to those of the Northern Hemisphere, which is consistent with the literature (e.g., Roemmich and Gilson, 2009). The weak extension in depth along the coast at the western boundaries in the Atlantic and Pacific marks the deep extension of the WBCs. The negative anomalies in Free-minus-Argo 1000/2000 SH differences indicate that the deep extension in depth of the gyres of the Southern Hemisphere and that of the WBCs are too weak in PSY4 Free compared with the SCRIPPS Argo product. These main patterns disappear in the Oper-minus-Argo 1000/2000 SH differences (Fig. 7d).

Finally, we provide a comparison of the meridional transport of the Atlantic meridional overturning circulation (AMOC), which plays a key role in controlling the climate system (Knight et al., 2005). In Fig. 8, the meridional transport at 26° N in the Atlantic from PSY4 Oper and PSY4 Free is obtained by integrating the meridional velocity in the upper 1200 m across the Atlantic (Balmaseda et al., 2007), and compared with the estimation deduced from the RAPID array (Cunningham et al.,

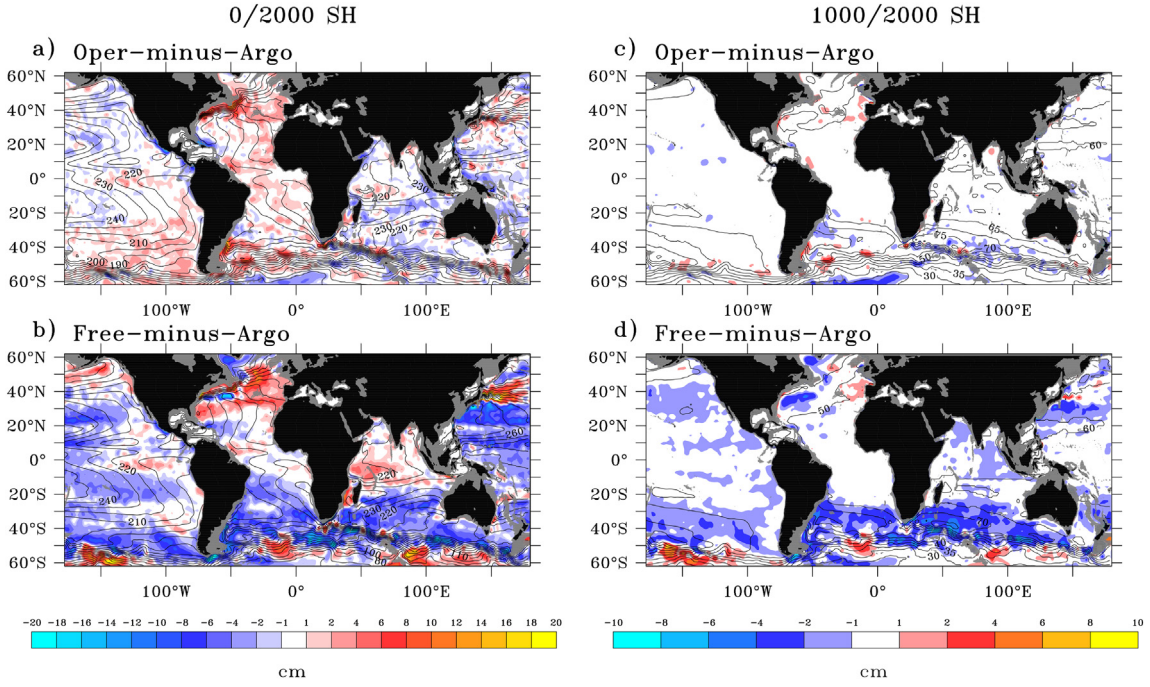

Fig. 7. (a) Steric height of the sea surface relative to 2000 m for PSY4 Oper annual means (contours), and Oper-minus-Argo differences (color shading). (b) Same except for PSY4 Free. (c, d) Same as (a, b), except for the 1000/2000 m SH. PSY4 and Argo fields are considered for the period 2007–2015. Unit is in dyn cm. (For interpretation of the references to color in this figure legend, the reader is referred to the web version of this article.)

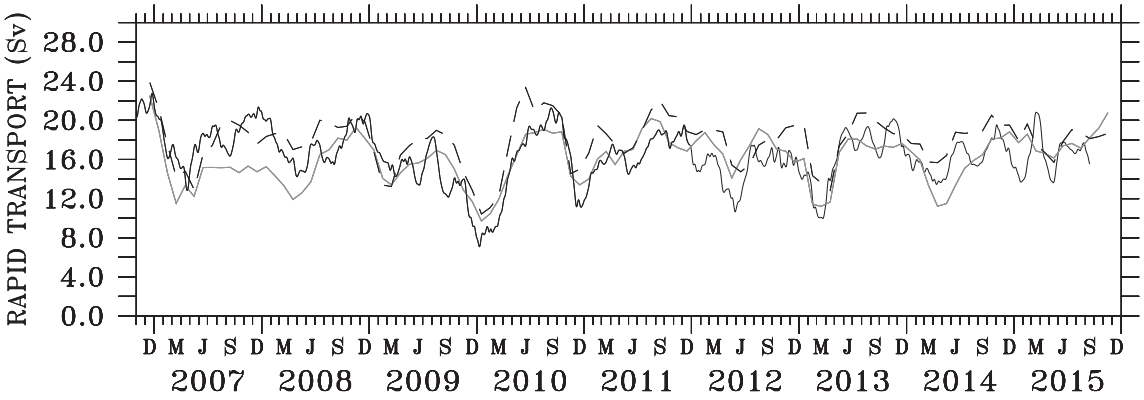

Fig. 8. Meridional transport at 26° N in the Atlantic, from the RAPID array (solid black, Florida straits + Ekman + upper mid-ocean transports), PSY4 Oper and PSY4 Free (respectively dashed black and gray lines, corresponding to the 0–1200 m meridional transport). Unit is in Sverdup (1 Sv = 10^6 m^3/s). Time series have been filtered using a 3-month running mean.

2007, downloaded from the http://www.rapid.ac.uk/). As mentioned previously, the velocity variables are not directly constrained in PSY4 Oper. For the period 2007–2015, the time-mean AMOC is estimated at 16.3 Sv (= 10^6 m^3/s) and 18.3 Sv for the PSY4 Free and PSY4 Oper respectively, suggesting that data assimilation increases the AMOC by 2 Sv. Compared with the RAPID estimation of 16.2 Sv, the PSY4 Free estimate appears thus to be more consistent with observations than PSY4 Oper. The choice of 1200 m as the depth of maximum overturning in the model, as well as the complex bathymetry in the Florida Strait, would require further investigations in order to accurately assess the time-mean AMOC in PSY4 Free and PSY4 Oper (Stepanov et al., 2012). However, the AMOC interannual variability is better represented by PSY4 Oper than PSY4 Free, with a correlation with RAPID time series of 0.66 for PSY4 Free and 0.76 for PSY4 Oper. These encouraging results will motivate further diagnostics in the subpolar gyre and in the south Atlantic with the implementation of the *Overturning in the Subpolar North Atlantic Program (OSNAP)* and the *South Atlantic MOC Basinwide Array (SAMBA)*.

In general, the large-scale features of the upper 2000 m temperature and salinity fields are well-reproduced by the PSY4 fields. Without data assimilation, the depth gradient of the thermocline or the tilt of subtropical gyres can differ from the SCRIPPS Argo product, thus generating substantial anomalies. Data assimilation plays a key role in correcting the position of the WBCs. The monitoring and forecasting system appear to consistently capture the large-scale patterns of the 2007–2015 mean states.

4. The 2007–2015 oceanic variability

In order to inform on the variability embedded in monthly PSY4 fields, the amplitude and phasing of the total-resolved signal are detailed with respect to two standard observational data sets. In Fig. 9a, the standard deviations of the monthly PSY4 Oper and PSY4 Free SSH fields shown were zonally-averaged and compared with the DUACS estimates for the period 2007–2015 to show the latitude dependence of the variability. The zonally-averaged amplitude of the SSH signal is generally around 6–7 cm, with a maximum of 11 cm at 35° N reflecting the variability of WBCs in the Northern Hemisphere. The consistency between DUACS and PSY4 Oper is evident, while PSY4 Free mostly differs on the meridional position of the maximum at 35° N related to the position of the WBCs as seen in Section 3. In Fig. 9b, the zonally-averaged correlation of DUACS with PSY4 Free (0.9 at the equator and decreasing below 0.6 near the poles) and PSY4 Oper (> 0.9 at almost all latitudes) demonstrates how data assimilation significantly changes the temporal phasing of PSY4 that it matches the DUACS altimetric product better.

Similarly to SSH, Fig. 9c shows the zonally-averaged standard deviations of the monthly PSY4 Oper and PSY4 Free fields, but for the 0/2000 SH, and compared with the SCRIPPS Argo estimates. Although the latitude dependency of the 0/2000 SH variability is closely consistent with that of SSH, the amplitude of the 0/2000 SH variability is slightly lower (~5–6 cm) to that of SSH. This is due to the variability of the deep SH (below 2000 dbar) and/or mass-related components, both of which are not included in the 0/2000 SH, but are in SSH. As for SSH, the latitude dependence of PSY4 Oper is more consistent with the observation data set than with PSY4 Free. However, unlike SSH, the amplitude of the 0/2000 SH from the SCRIPPS Argo product is slightly lower to that of PSY4 Oper and PSY4 Free and the correlation of the 0/2000 SH PSY4 Oper and PSY4 Free with the Argo product does not show large improvement as compared with SSH. These characteristics are mostly due to the small-scale variability (e.g., mesoscale activity), embedded in PSY4 fields, but not in the SCRIPPS Argo product (Roemmich and Gilson, 2009). Note that these results are not dependent on the choice of the Argo product, since the comparison with the French *In Situ* Analysis System (ISAS) Argo product (Kolodziejczyk et al., 2017) gives the same results. The consistency of the 0/2000 SH between PSY4 fields with Argo products is increased, when the small-scale variability is filtered out by using a 3 ° × 3° running mean (dotted line in Fig. 9d). However, the weaker consistency of the 0/2000 SH in comparison to that of SSH might be explained by the irregularly distributed Argo observations, which involve local errors (in both the Argo product and PSY4) due to data gaps in space and time.

4.1. The annual cycle

4.1.1. Temperature and salinity

Fig. 10a shows the zonally-averaged amplitude of the annual cycle temperature stratification for the upper 100 m layer ($T_{100m} - T_{surface}$) from PSY4 Free, PSY4 Oper and the SCRIPPS Argo product. The three fields consistently represent the strong hemispheric asymmetry, with a higher maximum seasonal temperature change in the Northern Hemisphere around 40° N (> 8°C) than in the Southern Hemisphere where the amplitude does not exceed 6 °C. As noted by Roemmich and Gilson (2009), air-sea flux and ocean heat advection associated with WBC dynamics can contribute to the pronounced asymmetry in seasonal change of temperature. The main differences concern the maxima amplitude in the tropics and in the Northern Hemisphere, which is closer to Argo in the PSY4 Oper than in the PSY4 Free fields. In the 100–300 m layer, the comparison of PSY4 Oper and PSY4 Free indicates that data assimilation has a significant impact on the representation of the variability in the tropical band, similarly to the SCRIPPS Argo product.

Fig. 11 shows the September-minus-March SSS differences for PSY4 Free, PSY4 Oper and the SCRIPPS Argo fields. The main SSS changes are

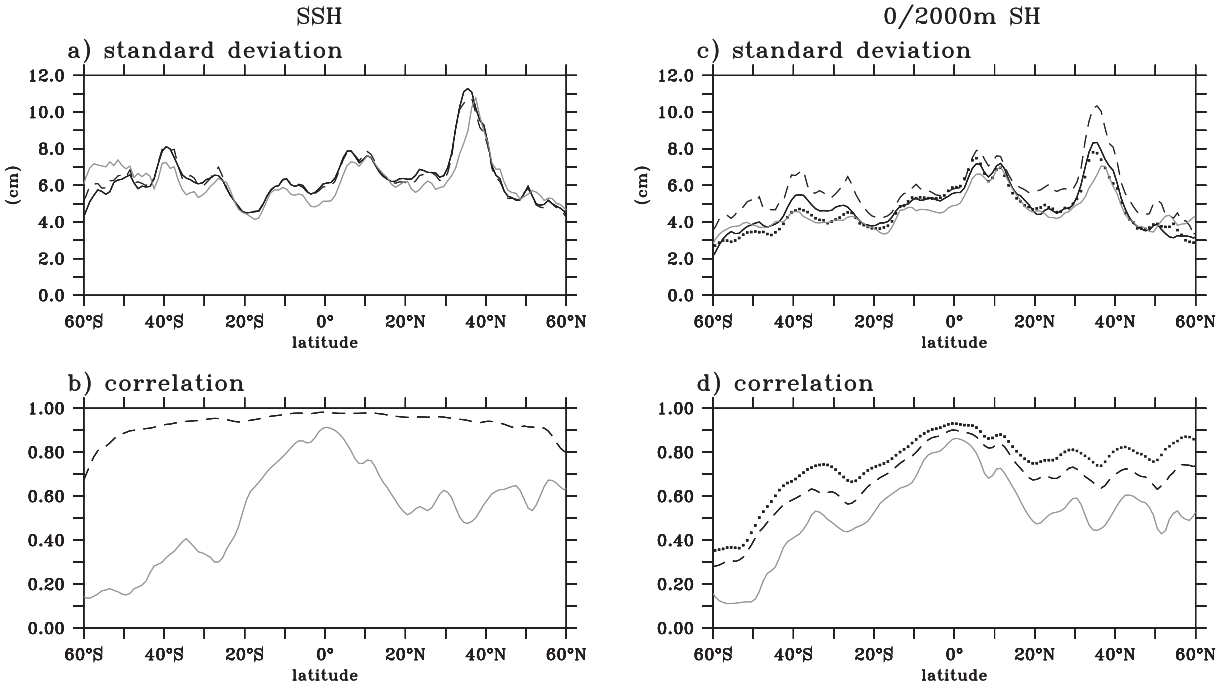

Fig. 9. (a) Zonally-averaged standard deviation (cm) of monthly SSH for the period 2007–2015 from the DUACS altimetric product (solid black line), PSY4 Oper (dashed black line) and PSY4 Free (gray line). (b) Zonally-averaged correlation of the DUACS altimetric product with PSY4 Oper (dashed black line) and PSY4 Free (gray line). (c–d) Same as (a–b), except for the 0/2000 SH and using the SCRIPPS Argo product as the observational data set. In (d), the dotted line indicates the correlation, after applying a 3° × 3° running mean.

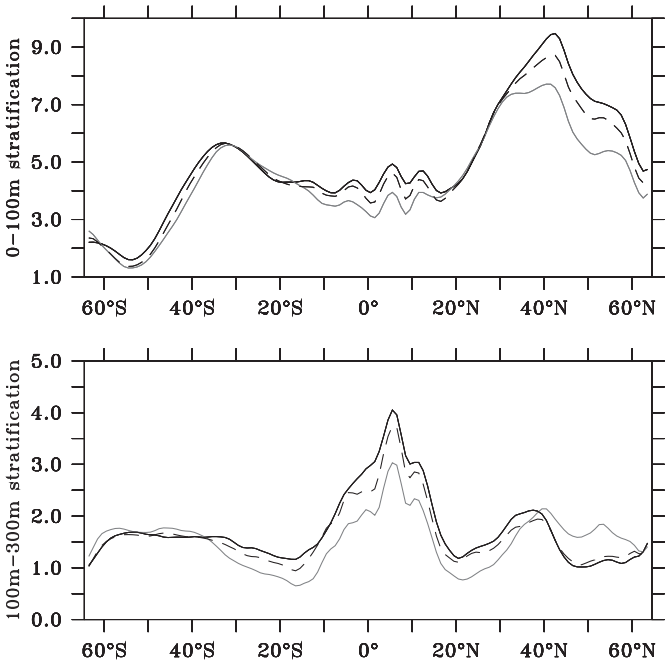

Fig. 10. (a) Zonally-averaged amplitude of the annual cycle (maximum minus minimum) of temperature stratification in the 0–100 m layer ($T_{100m} - T_{0m}$) for Argo (solid black), PSY4 Oper (dashed black) and PSY4 Free (gray). (b) Same except in the 100–300 m layer. Units are in °C.

observed in the tropical band. In the Atlantic and Pacific, zonal structures reflect precipitation changes, through the meridional position of the Intertropical Convergence Zone and the South Pacific Convergence Zone. Positive anomalies along the equator indicate higher salinity in September than in March, when the ITCZ is located at its southernmost position and when the SPCZ has reached its seasonal intensity (Brown et al., 2011; Yu, 2011). In the Indian Ocean, positive anomaly patterns are associated with processes related to the seasonal monsoon and horizontal advection (Donguy and Meyers, 1996; Rao and Sivakumar, 2003). Thus, annual changes of SSS in PSY4 Oper and PSY4 Free appear to be well-consistent with the SCRIPPS Argo product.

4.1.2. Sea surface height

Fig. 12 shows the September-minus-March SSH differences from the DUACS altimetric product, PSY4 Oper and PSY4 Free fields. A clear hemispheric asymmetry is seen, with higher SSH in September (boreal summer) than in March (boreal winter) in the Northern Hemisphere, and the opposite in the Southern Hemisphere. The higher amplitude of the Northern Hemisphere (> 5 cm) compared with that in the Southern Hemisphere (~5 cm) is consistent with the annual temperature variability described in Fig. 10a, which demonstrates the critical role of the upper-ocean temperature in the annual variability of SSH. The highest amplitude is found in the WBC regions and along the tropical band, where September-minus-March SSH differences are characteristic of westward-propagating annual Rossby waves (Gasparin and Roemmich, 2017). These global seasonal patterns are well-reproduced in the PSY4 fields, except in WBC of PSY4 Free, in which the main energetic structures are not correctly positioned as mentioned previously. Thus, SSH variability appears to be consistent with the DUACS altimetric product at annual time scales. A similar conclusion can be made about the 0/2000 SH quantity compared with the SCRIPPS Argo product.

4.2. The long-term variability

4.2.1. Ocean heat content

The quality of PSY4 fields for representing oceanic variability was also assessed by comparing the PSY4 ocean heat gain over the 0–2000 m layer with that of the SCRIPPS Argo product. Based on the same observation product, Roemmich et al. (2015) have shown a continued increase of the ocean heat content in the upper 2000 m over the period 2006–2013. They showed that most of the increase occurs in the Southern Ocean, but that some regional trends can exceed ± 10 W/m^2

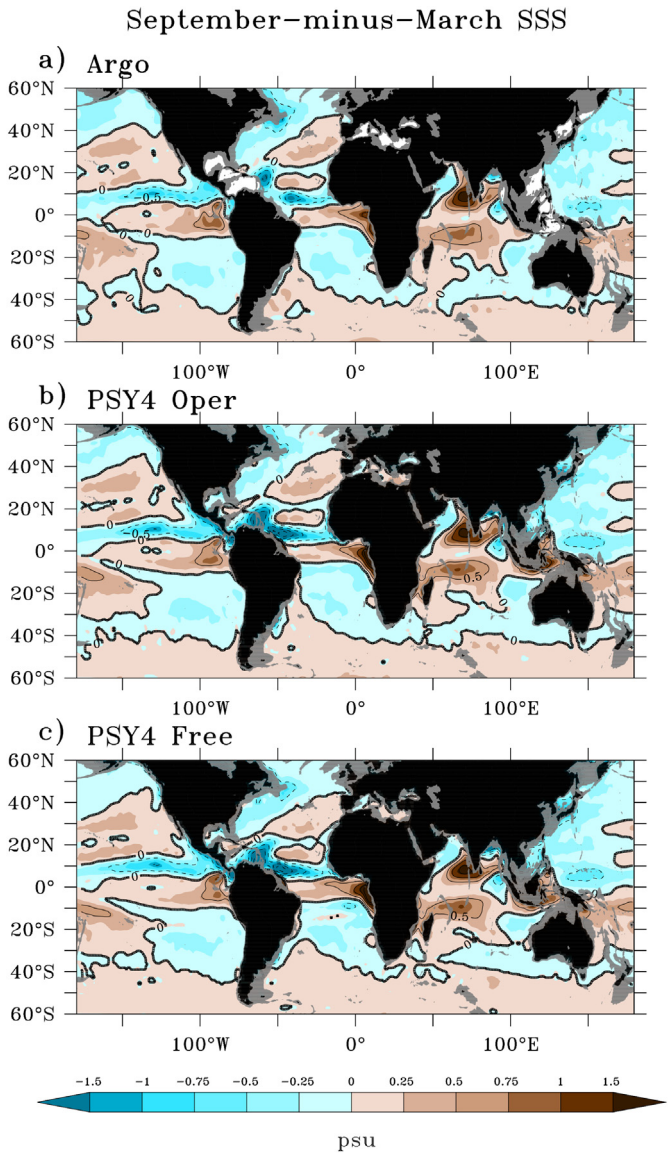

Fig. 11. September-minus-March SSS from (a) Argo, (b) PSY4 Oper, and (c) PSY4 Free. Unit is in psu.

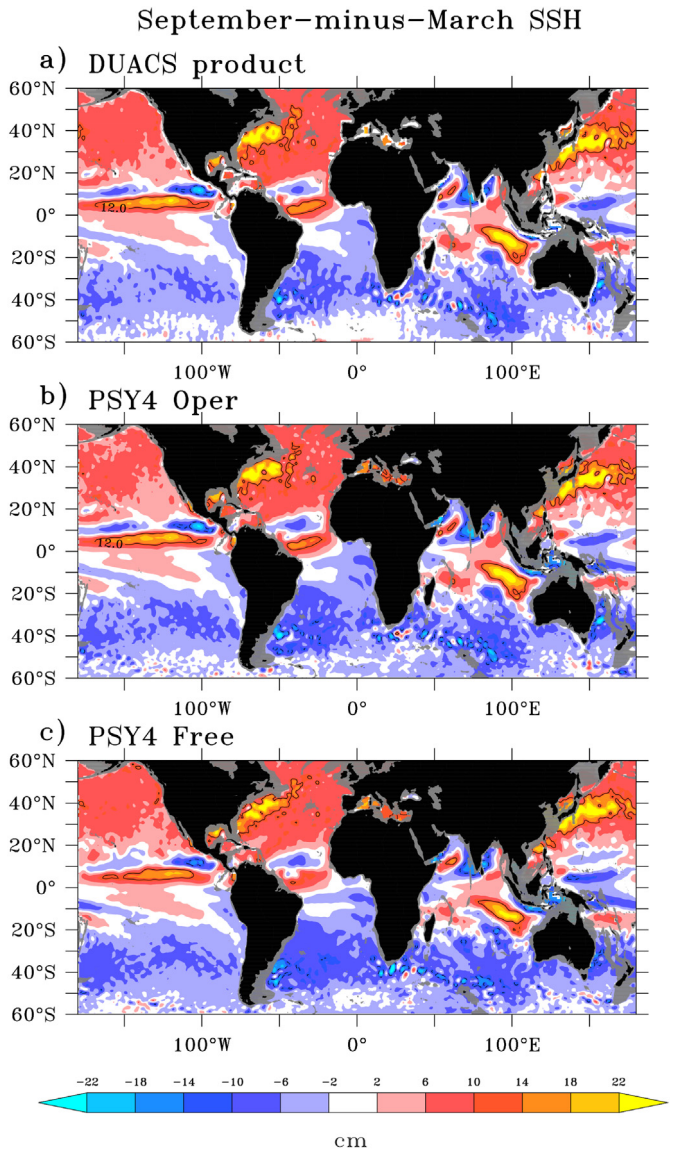

Fig. 12. September-minus-March SSH differences from (a) DUACS, (b) PSY4 Oper, (c) PSY4 Free. The black line indicates the 12 cm-isoline. Unit is in dyn cm.

in the WBCs of the Northern Hemisphere. By comparing our results with the same observation product, the aim was to evaluate the consistency of the PSY4 fields in representing the spatial structures of the ocean heat content changes for the period 2007–2015. Note that the analysis of the 2007–2015 deep ocean variability is limited in PSY4 Free fields due to the need to adjust the dynamic model following its initialization in October 2006.

In Fig. 13, the 0–2000 m heat gain changes deduced from the SCRIPPS Argo product, PSY4 Oper and PSY4 Free show clear spatial distribution with a significant warming in the central-eastern Pacific and cooling in the far western basin. This illustrates the large influence of interannual variability during the period 2007–2015, which was marked by a strong El Niño event in 2015 (Von Schuckmann et al., 2016). This specific pattern, not seen in Roemmich et al. (2015) who calculated ocean heat content changes over the 2006–2013 period, illustrates the large uncertainty in the trend over a short time-interval, including interannual and decadal variability. Besides this tropical variability, most of the signal is located at mid-latitudes around 40 °, with important discrepancies in PSY4 Free as compared to PSY4 Oper and the SCRIPPS Argo product. Positive trends observed at mid-latitudes in the Southern Hemisphere are not as clear in PSY4 Free, which shows strong negative trends at the south of Africa. In addition, strong positive trends in PSY4 Free are seen in the subpolar North Pacific and North Atlantic, but not in PSY4 Oper and the SCRIPPS Argo product. In the subtropical Atlantic, a positive trend is only seen in PSY4 Oper, and potentially results from the assimilation of SLA and a reduced number of *in situ* observations at the beginning of the period. In general, PSY4 Oper shows consistent regional patterns with the SCRIPPS Argo product, but the amplitude of the PSY4 Oper can be regionally twice as high as than the SCRIPPS Argo product. Note that uncertainties as to long-term trends derived from Argo can be great on a regional level (Von Schuckmann and Le Traon, 2011). Thus, although this demonstrates the significant contribution of the current integrated observing system for representing the 2007–2015 ocean heat content trend in the Mercator system, important differences between PSY4 Oper and Argo estimates suggest that some progress still needs to be made to improve representation of the long-term variability of such an integrated quantity.

Having considered some critical aspects of the upper-ocean variability from PSY4 fields and the SCRIPPS Argo product, we focus here on the model's unique contribution to providing homogeneous estimation

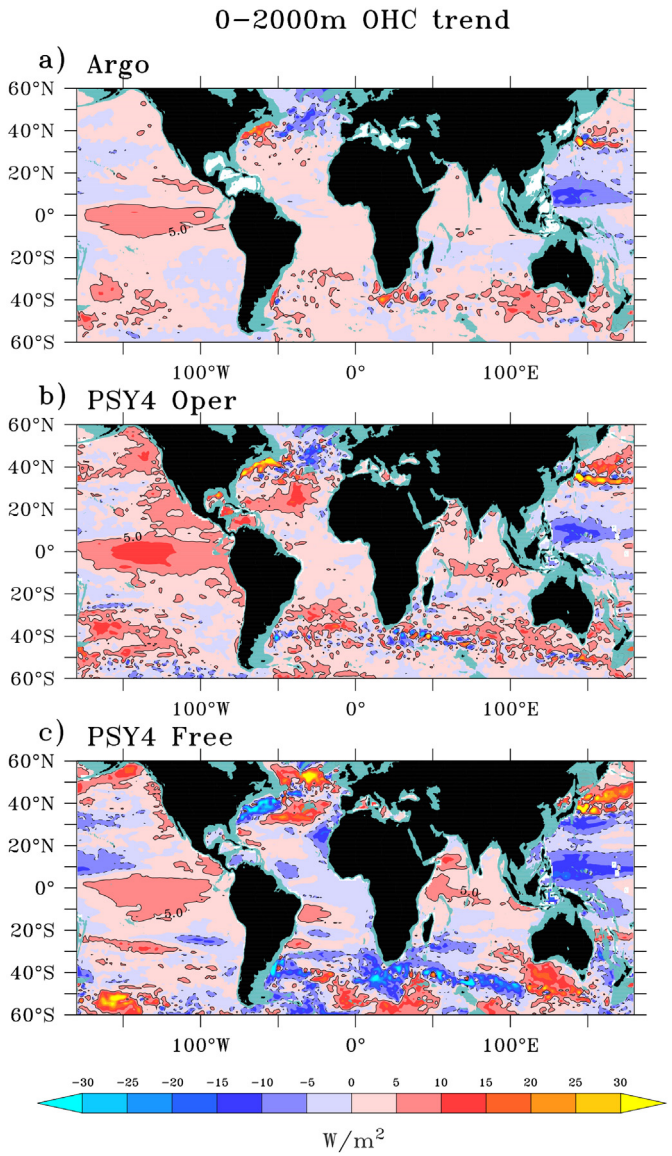

Fig. 13. 0-2000 m ocean heat content trend for the period 2007–2015 from (a) Argo, (b) PSY4 Oper, and (c) PSY4 Free. Unit is in W/m^2.

of deep ocean variability. Due to the large number of unresolved issues with deep ocean processes and given that there are not very many deep ocean observations available, only a few studies based on models have investigated deep ocean variability (e.g., Kouketsu et al., 2011). Fig. 14 shows the 9-yr trend of the ocean heat content for the layers 2000–4000 m (deep basin), and 4000–6000 m (abyssal basin) within 32 deep/abyssal ocean basins around the globe (Purkey and Johnson, 2010). Consistently with estimations made by Desbruyères et al. (2016, see their Fig. 3) and Purkey and Johnson (2010), who mainly used repeated hydrographic surveys, the spatial distribution of trends in both PSY4 fields is characterized by a strong warming in the Southern Ocean (in the deep and abyssal oceans), with some basins exceeding 1 W/m^2. The distribution and amplitude of large-scale changes are broadly consistent with the literature. However, differences with literature can be fairly great on a regional scale. For instance, the strong cooling in the Indian Ocean is not seen in the estimations of Desbruyères et al. (2016) or Kouketsu et al. (2011). The cooling in the North Pacific Ocean appears strong compared with previous studies. An important aspect of the PSY4 system concerns the assimilation of deep climatological profiles in PSY4 Oper, as described in Lellouche et al. (2018). This technique prevents from unrealistic deviation of the PSY4 Free in specific regions such as in the southern Indian Ocean and the southern Atlantic (e.g., Fig. 14c, d). Thus, significant uncertainties remain as to the representation of deep ocean variability from PSY4 fields, whose deep ocean is not yet constrained by deep observations, unlike the upper-ocean. Thus, even though large-scale patterns appear to be quite consistent with the literature, the on-going development of the deep ocean observing system should significantly reduce uncertainty in long-term variability of the deep ocean and increases the ability of monitoring and forecasting systems to consistently represent deep ocean variability (Johnson et al., 2015).

4.2.2. Ocean freshwater content

The ocean freshwater content is deduced by vertical integration of the salinity anomaly, representing the amount of freshwater needed for the observed dilution (about 3 cm of freshwater are needed to dilute 1 m of seawater by 1 psu). In Fig. 15a, the spatial distribution of ocean freshwater content trend in the upper 2000 m from the SCRIPPS Argo product exhibits large-scale patterns in the three oceans, with a stronger amplitude in the North Atlantic and in the Southeast Indian basins. While PSY4 Free fields show very different patterns, the basin-scale signals observed in Argo are also seen in PSY4 Oper, and are similar to that of the halosteric component of the sea level trend of Llovel and Lee (2015, their Fig. 1d) and Wang et al. (2017, their Fig. 3a). They explain these halosteric patterns in the Southeast Indian by increased precipitation in the Indonesian seas plus ocean dynamics. In addition, Wang et al. (2017) suggest that the meridional overturning circulation in the North Atlantic, related to the North Atlantic Oscillation (NAO), would impact on the vertical mixing of salinity and halosteric changes, demonstrating the role of ocean dynamics in addition to surface forcing. Similarly to ocean heat content trends, the PSY4 Oper has the same patterns, with stronger amplitude as the SCRIPPS Argo product.

4.2.3. Sea surface height and 0/2000 steric height

To further explore the long-term variability of the upper-ocean in PSY4 fields, the zonally-averaged 0/2000 SH, plus the thermosteric and halosteric components, are detailed in Fig. 16 for the SCRIPPS Argo product, PSY4 Oper and PSY4 Free. The halosteric component in SH is estimated by subtracting SH, with salinity replaced by the 2007–2015 mean value, from SH with the observed salinity included (Maes et al., 2002). The thermosteric component is deduced in a similar way. The latitude dependence of steric trends in the SCRIPPS Argo product is globally consistent with Levitus (2005, their Fig. 1), although our analysis was performed for a shorter period resulting in higher amplitude trends resulting from interannual and decadal variability (e.g. in the tropical band). Most of the steric changes are controlled by the thermosteric component, except north of 40° N where large halosteric contributions occur in the Pacific and Atlantic oceans (Levitus, 2005). Consistently with previous results, steric trends in PSY4 Oper have the same general patterns as the SCRIPPS Argo product, with a similar halosteric contribution north of 40° N, but with higher amplitude trends. In addition to progress in modeling and surface fluxes, the comparison with PSY4 Free estimates, which are significantly different from PSY4 Oper, reinforces the critical need for data assimilation in order to represent the long-term variability of such integrated quantities.

Even though regional differences of PSY4 in comparison to observation data sets can probably cause significant differences in globally-averaged quantities, closing the globally-averaged sea surface height balance is fundamental for monitoring the climate system. Table 1 shows the globally-averaged linear trends of SSH and 0–2000 SH from PSY4 fields and observation data sets for the period 2007–2015. Several points are worth noting. First, the globally-averaged SSH trend from altimetry is estimated at 4.0 mm/yr, which is significantly higher than the quite stable SSH trend of around 3 mm/yr from the last 20 years (Chambers et al., 2016). This is attributed to the large interannual variability related to the occurrence of the strong

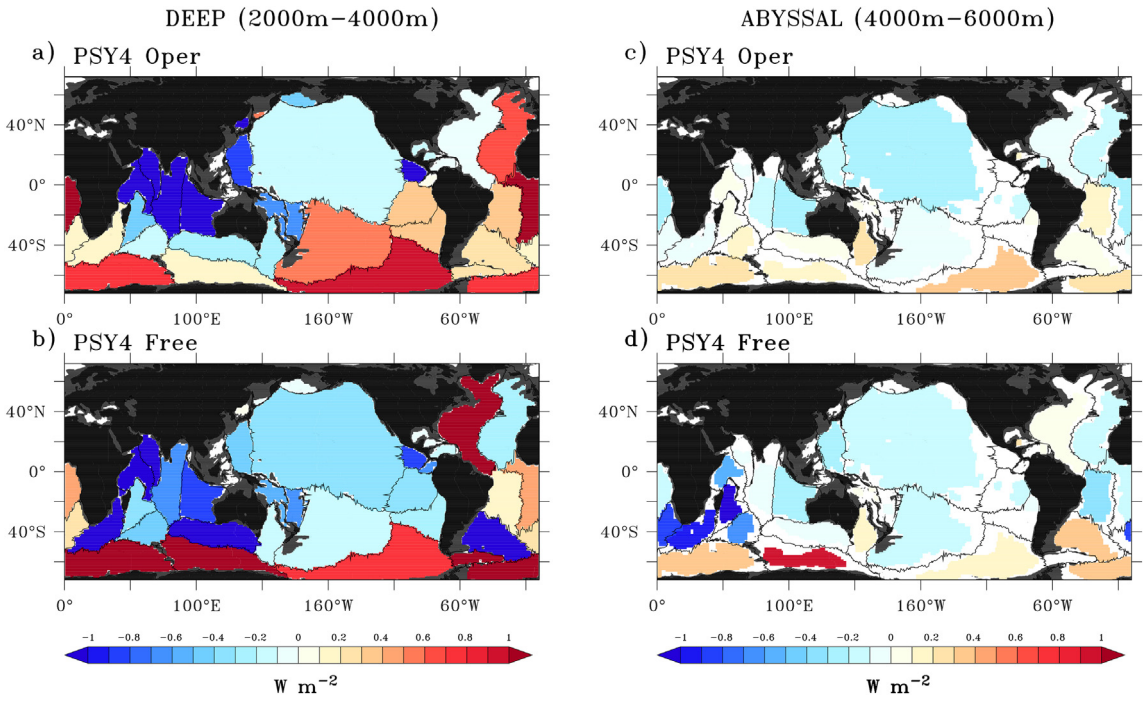

Fig. 14. (a, b) Deep ocean heat content trends for the layer 2000 m–4000 m from (a) PSY4 Oper and (b) PSY4 Free. (c, d) Same except for the layer 4000 m–6000 m. Unit is in W/m^2.

2015/2016 El Niño, since the same calculation done on the 2005–2014 period gives a trend of 3.1 mm/yr. The globally-averaged SSH trend deduced from observations is partly recovered by PSY4 Oper with an estimate of 3.2 mm/yr (representing 80% of the DUACS trend), while PSY4 Free has a SSH trend of only 1.8 mm/yr (45% of the DUACS trend). One possible interpretation of why PSY4 Oper does not capture the global SSH trend completely lies in the errors in the MDT, identified as the dominant source of error in sea level (Haines et al., 2011). Systematic errors in the MDT fields result in sequential regional warming/cooling at each 7-day cycle. These warming/cooling artifacts are only partly corrected by the bias correction, and thus, can impact on the representation of the time variability (Drecourt et al., 2006; Lea et al., 2008). Despite specific corrections, uncertainties on the global freshwater budget can also involve a mean sea surface height drift (Lellouche et al., 2013). Second, the globally-averaged 0/2000 SH trends show the distinctive characteristics of SSH trends. The SCRIPPS Argo product gives an estimate of 1.3 mm/yr for the period 2007–2015 (1.0 mm/yr for the period 2004–2015, Chambers et al., 2016). Surprisingly, PSY4 fields provide a significantly different 2007–2015 globally-averaged trend to the Argo estimate. While PSY4 Free fields gives a 2007–2015 negative trend of −1.0 mm/yr, PSY4 Oper shows a too strong trend of 2.8 mm/yr. Thus, the globally-averaged long-term variability of PSY4 Oper is under-estimated for the SSH, but over-estimated for the 0/2000 SH. These results demonstrate that recovering a long-term signal remains challenging for a monitoring and forecasting system.

4.3. Monitoring the global ocean: the case study of the El Niño anomalies in the tropical North Pacific in 2014/2015

As shown previously, the PSY4 operational system is able to capture most of the large scale variability in the latitude band between 65° S and 65° N. In order to illustrate how such systems can be used to answer relevant scientific questions, this issue is further investigated by using as a case study the northward pathways of El Niño anomalies in the tropical North Pacific. As a supplement to the study of Hasson et al. (2018, see their Fig. 5), we focus on the 2014 and 2015 years because they present distinctively different SSS features in the topical North Pacific in relation to the El Niño-Southern Oscillation (ENSO). In early 2014, several oceanic and atmospheric apparently have suggested the onset of an El Niño event, but easterly wind events in mid-2014 have probably stopped the development of the on-going event (Hu and Fedorov, 2016). In 2015, the onset of the 2015/2016 El Niño led to a large equatorial freshwater anomaly, with extensive spatial and large amplitude characteristics (Gasparin and Roemmich, 2016).

In Fig. 17, the SSS anomaly, calculated by subtracting the monthly climatology, is shown in April and October for the years 2014 and 2015 from PSY4 Oper and the SCRIPPS Argo product. In general, the main features described by Hasson et al. (2018) are found in the PSY4 Oper fields. In April 2014, the SSS fields in PSY4 Oper are marked by a negative anomaly (< 0.5 psu) along the equator west of the dateline. From April to October 2014, this SSS anomaly moves further west, and extends northeastward as far as the eastern Pacific in a large latitude band between 5° N and 10° N. In April 2015, the SSS conditions differ mainly from April 2014 conditions by the presence of a negative anomaly, which extends from the western to the eastern Pacific in the latitude band between 5° N and 15° N. In October 2015, the fresh SSS anomaly is characterized by its high amplitude, in both the western equatorial part and in the latitudinal band around 5° N. The comparison with the SCRIPPS Argo product (Fig. 18e–h) shows consistent basin wide features, with a slightly smaller amplitude than that in PSY4 Oper.

In addition to the SSS anomaly, the near-surface currents and the net freshwater surface flux, which forces the model, are provided by the PSY4 Oper system and are superposed on the SSS anomaly (Fig. 17 a–d) in order to discuss the processes involved in the observed SSS variability. In April 2014, while the NECC is relatively weak, the net surface freshwater flux under the ITCZ appears significant. In October 2014, the NECC is intensified and its position clearly corresponds to the position of the SSS anomaly. This supports the results of Hasson et al. (2018), stating that both horizontal advection and freshwater flux contribute to the SSS anomaly in October 2014. In April 2015, the fresh SSS anomaly is more significant than in April 2014, which mainly results from the preconditions of 2014 and the on-going development of the 2015/2016 El Niño (Gasparin and Roemmich, 2016). In October 2015, both the

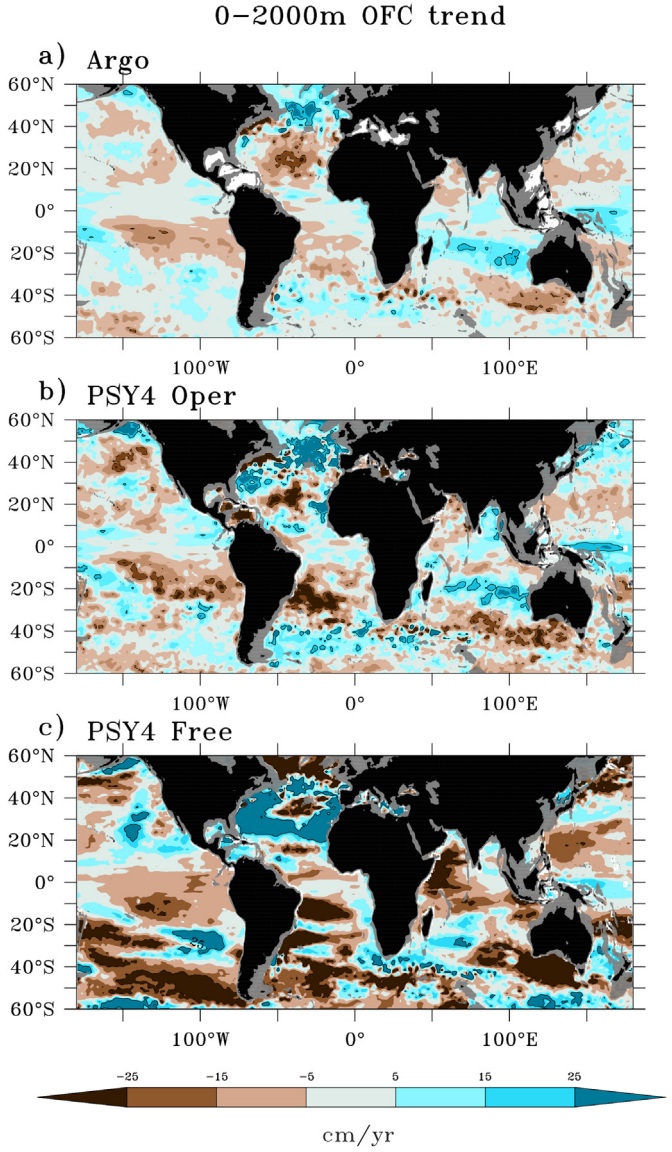

Fig. 15. 0–2000 m ocean freshwater content trend for the period 2007–2015 from (a) Argo, (b) PSY4 Oper, and (c) PSY4 Free. The solid black line indicates the isoline 25 cm/yr, while the dashed line is the −25 cm/yr isoline. Unit is in cm/yr.

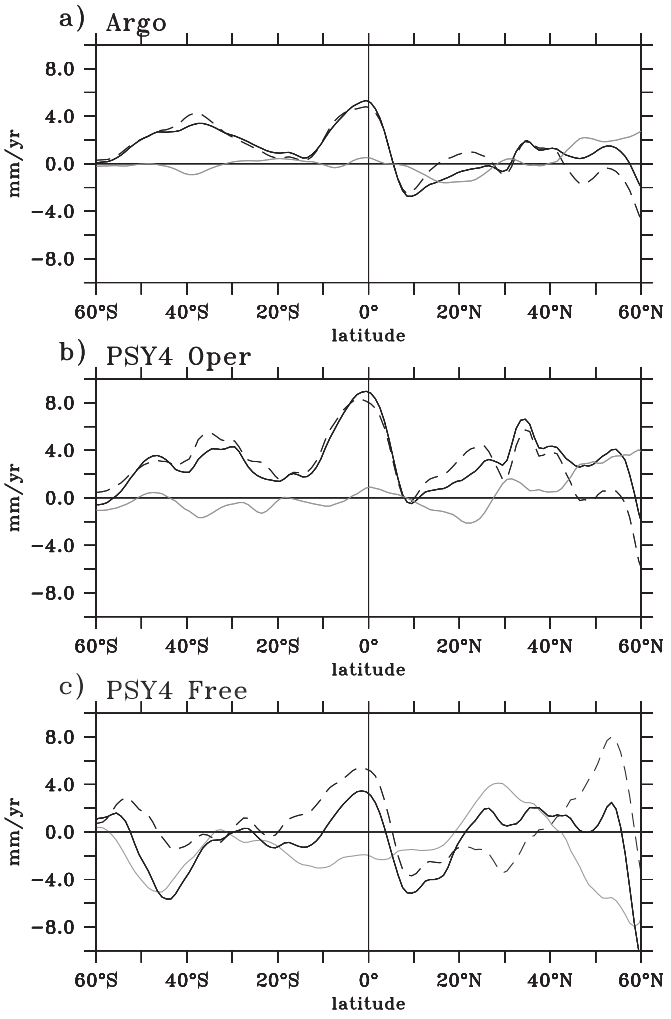

Fig. 16. Zonally-averaged trends over the period 2007–2015 of steric (solid black line), thermosteric (dashed black line) and halosteric (gray line) components for the 0–2000 m upper-ocean from (a) Argo, (b) PSY4 Oper, and (c) PSY4 Free. Unit is in mm/yr.

NECC and the net freshwater flux are much stronger than in 2014, which is in line with the results of Hasson et al. (2018). Though further investigations are needed for quantitatively estimate the contribution of each process involved in the freshwater budget, the present description demonstrates the unique skill of the high resolution PSY4 operational system for providing consistent physical oceanic conditions (i.e., temperature, salinity, velocity fields, sea surface height) as compared with a multi-product analysis.

In Fig. 18, the salinity anomaly is also shown in vertical sections in the upper 300 m averaged between 5° N and 10° N, with the absolute current velocity, including zonal and vertical components, superposed on the salinity anomaly. In Fig. 18a, the fresh anomaly observed in April 2014 extends to about 60 m depth, and is advected eastward by the NECC in October 2014. Note that the zonal component dominates. As mentioned previously, the salinity conditions in April 2015 (Fig. 18c) are characterized by fresh waters located further east, which extend deeper (~100 m). As compared to October 2014, the stronger contribution of the NECC clearly appears in October 2015, especially around 140° W, where the larger freshwater anomaly is seen (with

Table 1
Globally-averaged trend (60° S–60° N) in SSH and 0/2000 SH for the period 2007-2015. Observations are deduced from the altimetric DUACS product for SSH estimates, and the SCRIPPS Argo product for 0/2000 SH estimates.

	SSH	0/2000 SH
2007–2015		
Observations	4.0	1.3
PSY4 Free	1.8	−1.0
PSY4 Oper	3.2	2.8
2005–2014		
Chambers et al. (2016)	3.2	0.9

values lower than −0.8 psu). In general, PSY4 Oper shows stronger signal and smaller-scale patterns than the Argo product, and this can potentially be explained by the smoothing of the interpolation procedures of the Argo product (Roemmich and Gilson, 2009). As mentioned by Hasson et al. (2018), small-scale currents could play a significant role in the northward advection of the salinity anomaly in this region, but their model was too smooth to resolve small scale eddies due to its 1° horizontal resolution at 20° N. Thus, the different parameters involved in the main processes involved in freshwater budget in 2014 and 2015 are represented with unprecedented details by PSY4 Oper, allowing new questions to be raised, such as concerning the role of small-

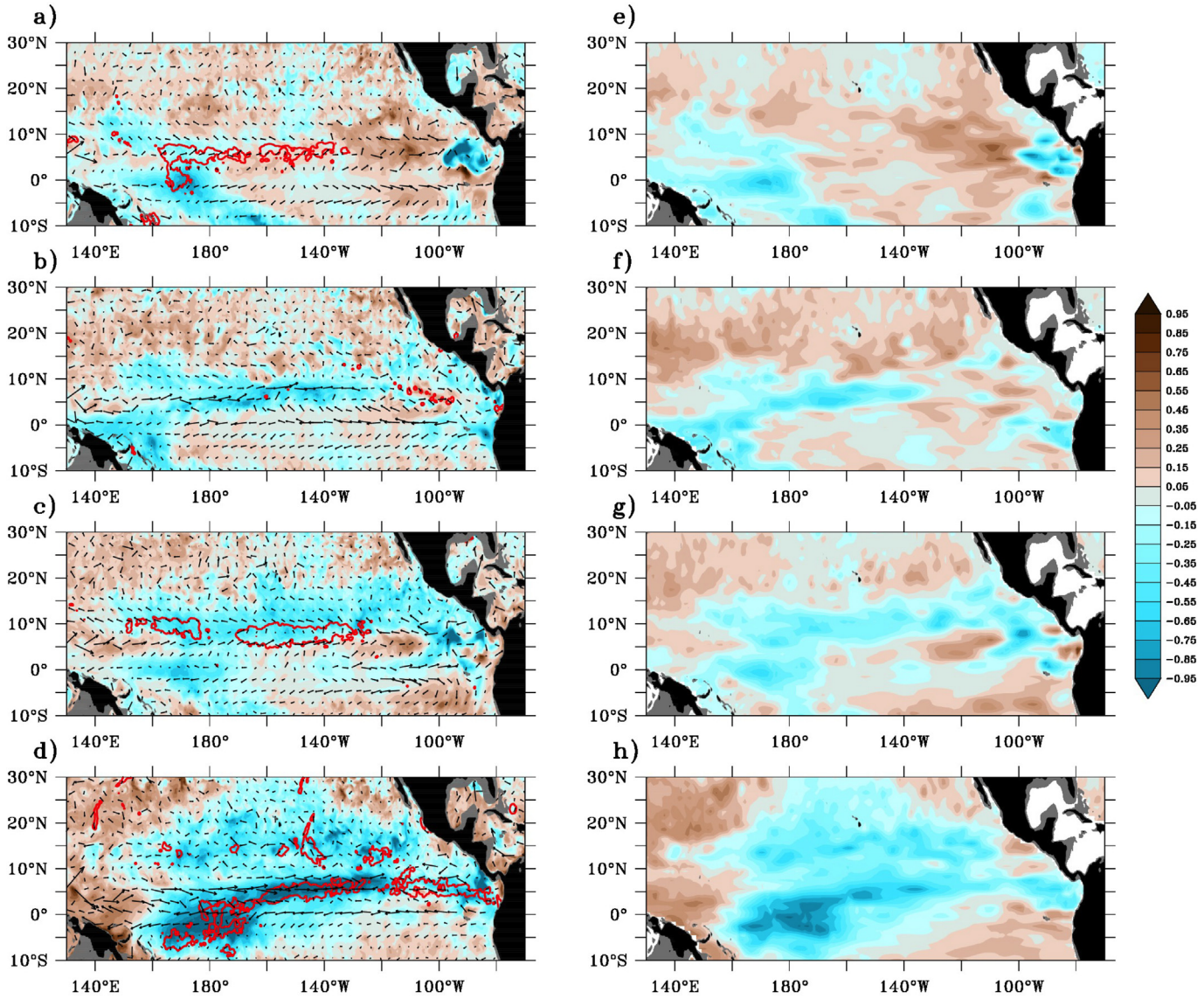

Fig. 17. Sea surface salinity anomaly (color shading) and absolute current velocity (arrows in a–d) for the months of April 2014 (a, e), October 2014 (b, f), April 2015 (c, g) and October 2015 (d, h) from PSY4 Oper (a–d) and the SCRIPPS Argo product (e–h). In (a–d), the red contour indicates the value of −2.5 mm/yr of the net freshwater flux. Anomalies are calculated from the climatological cycle. Units are in psu for salinity, and m/s for current velocity. (For interpretation of the references to color in this figure legend, the reader is referred to the web version of this article.)

scale and recirculation processes in the transport of salinity anomaly.

5. Conclusion and discussion

The study presents a detailed description of the large-scale variability embedded in the PSY4 global high resolution ocean monitoring and forecasting system of CMEMS. PSY4 monthly fields for temperature, salinity and SSH have been examined in order to assess the PSY4's ability to correctly represent the temporal mean, the annual cycle and the longer-term variability of the upper-ocean for the 2007–2015 period, and to demonstrate the impact of data assimilation in improving consistency with observation products based on a single instrument type. This 1/12° horizontal resolution monitoring system assimilates almost all of the information from satellites and multi-instrument *in situ* databases for providing weekly ocean forecasts and analyses at a global scale. A twin-free simulation without any assimilation of *in situ* and remote observations has been performed in parallel with the monitoring and forecasting system in order to evaluate the effective impact of the integrated ocean observing system. Compared with the previous 1/12° monitoring system at Mercator Océan, which was limited to a 3-yr period, these 11-yr time-series allow for more robust variability statistics.

A comparison of surface and subsurface fields demonstrates the critical role of observations for constraining model behavior in significantly reducing biases. At the surface, warm SST bias in upwelling regions and fresh SSS bias in the Amazon and Orinoco regions are strongly reduced in the monitoring and forecasting system in comparison to the twin-free simulation. The position of the main global structures, such as WBCs and subtropical gyres, has changed in agreement with observation data sets. In the subsurface, the depth gradient along the thermocline has globally increased, but work is still needed to improve representation of the upper-ocean thermal stratification, which remains too diffuse in comparison to the SCRIPPS Argo product. It is important to note that subsurface comparisons are constrained to the Argo's sampling, which does not include shallow waters and hardly represents energetic regions due to a low signal-to-noise ratio.

The monthly and longer-term variability of both PSY4 Free and PSY4 Oper simulations appears to be consistent with observations in

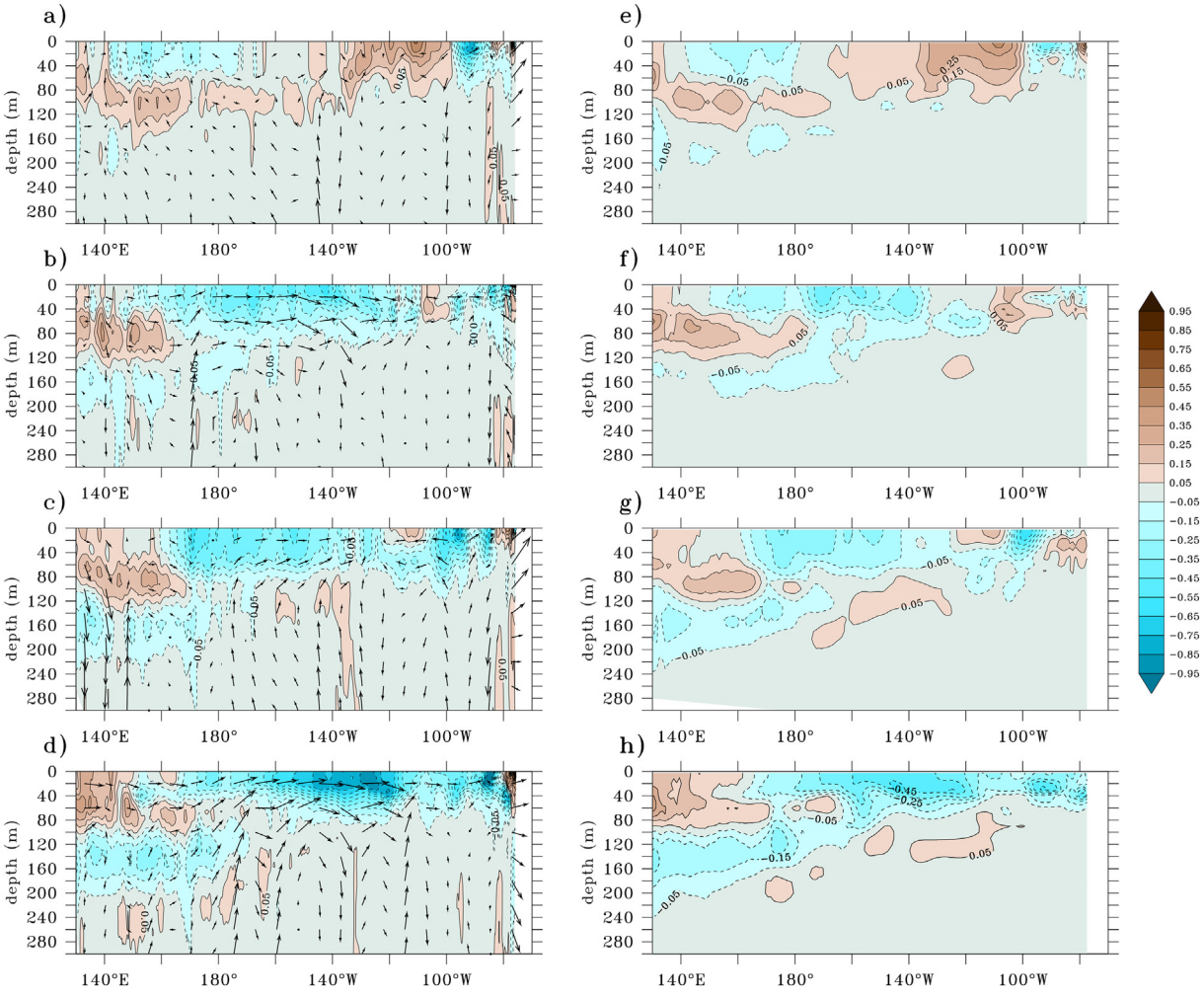

Fig. 18. Same as Fig. 17, but for subsurface salinity anomaly (color shading) and absolute current velocity (arrows), latitude-averaged over 5°–10° N in the upper 300 m. The current velocity has been vertically interpolated every 40 m. (For interpretation of the references to color in this figure legend, the reader is referred to the web version of this article.)

terms of amplitude. The PSY4 Free simulation does a good job of statistically representing basin-scale phenomena. This is of great interest for other research activities such as impact studies for observing system design. As an example, the PSY4 Free simulation presented here is at the basis of the common observing system experiments carried out in the framework of the AtlantOS project (Visbeck et al., 2015). Furthermore, biogeochemical forced-models could be based on this free simulation. Such study, which investigates long-term variability of an unconstrained simulation, is also of interest for coupled climate models.

Data assimilation is fundamental for phasing processes, both in space and time. Annual variability of temperature, salinity, SH and SSH appears to be consistent with observation data sets in both PSY4 estimates. The longer-term variability of ocean and freshwater content changes show similar regional patterns to the Argo product, but with a stronger amplitude regionally. Globally-averaged estimates of SH trend, including thermosteric and halosteric components, are too strong. Although significant progress has been made in representing the long-term variability of these quantities, some progress is still needed to better represent the amplitude of changes of such integrated quantities. Unlike the 0/2000 SH, SSH long-term variability PSY4 Oper is weaker in comparison to the DUACS product, showing that the SSH balance at these time-scales should be further investigated in the Mercator Océan system. The WBC regions in the Northern Hemisphere and the Southern Ocean are where the amplitude of ocean and freshwater contents (and 0/2000 SH) shows the highest difference compared with the observation product.

By comparing the monitoring and forecasting system with a twin-free simulation, the present work has demonstrated the striking improvements due to data assimilation, but has focused on the contribution of the global ocean observing system as a whole. Thus, further investigations are needed for identifying the respective role between the satellite and *in situ* components of the global ocean observing system. The *in situ* component, made up of a wide range of different instruments, is somewhat more complex than the regularly sampled altimetry observations. While significant efforts are being made to analyze the performance of the dynamic representation of the ocean by the current and future satellite constellation (Bell et al., 2015), our understanding of the *in situ* counterpart is less advanced and requires an accurate knowledge of each type of platform (Lea et al., 2014). Today, assimilation of the *in situ* information in the Mercator Océan system assigns the same instrument error regardless of the type of platform, meaning that the weight of an XBT profile is similar to that of an Argo profile. Even if the representativeness error (unresolved variability embedded in observation like internal-gravity waves) is larger than instrument error, the refining of assigned instrument errors in *in situ* observations should improve the impacts of *in situ* networks on the monitoring and forecasting system. The enhancement and extension of the observing networks to create an integrated observing system are carried out by combining scientific and operational needs, which should greatly benefit operational systems.

Besides significant improvements due to data assimilation of the ocean state representation, some model deficiencies still persist in the operational system. Further enhancements of the ocean observing system (e.g., sampling at the near-surface, into the deep ocean, in the WBCs), plus progress in assimilation schemes of current and future data sets (e.g., Satellite SSS, swath SST) should improve constraints on the operational system. In addition, several projected model developments in the NEMO3.6 version, including (i) a more sophisticated sea ice model with multi-categories, (ii) a higher vertical resolution of the ocean model, and (iii) improvements of vertical physics and advection schemes, should help to resolve issues related to important ocean processes, such as the ones occurring in the tropical thermocline or in the WBC regions.

In conclusion, the 11-yr time series of the global high resolution ocean monitoring and forecasting system PSY4 have modeled consistent large-scale variability at a global scale in comparison to observation products. This description of the PSY4 system will also be useful for the forthcoming eddy-resolving 1992–2016 reanalysis GLORYS (GLobal Ocean ReanalYsis and Simulation) at 1/12° horizontal resolution, which is based on the same PSY4 system. The main differences concern the reprocessed atmospheric forcing coming from the global atmospheric reanalysis Era-Interim (Dee et al., 2011) and a few changes in the system settings for observation errors. The main results of this paper could potentially be transferred to GLORYS estimates.

Acknowledgments

This study has been conducted using the Copernicus Marine Service Products. This paper uses data collected and made freely available by programmes that constitute the Global Ocean Observing System and the national programmes that contribute to it (http://www.ioc-goos.org/). This project has received funding from the European Union's Horizon 2020 research and innovation programme under grant agreement No.633211. We want to thank all Mercatoriens who contributed to the different stages from scientific and technical developments to users distribution of the monitoring and forecasting system. We also thank S. Purkey for providing the mask of deep ocean basins.

References

Amante, C., Eakins, B.W., 2009. ETOPO1 1 arc-minute Global Relief Model: Procedures, Data Sources and Analysis. US Department of Commerce, National Oceanic and Atmospheric Administration, National Environmental Satellite, Data, and Information Service, National Geophysical Data Center, Marine Geology and Geophysics Division Colorado.

Balmaseda, M.A., Hernandez, F., Storto, A., Palmer, M.D., Alves, O., Shi, L., Smith, G.C., Toyoda, T., Valdivieso, M., Barnier, B., 2015. The ocean reanalyses intercomparison project (ORA-IP). J. Oper. Oceanogr. 8, s80–s97.

Balmaseda, M.A., Smith, G.C., Haines, K., Anderson, D., Palmer, T.N., Vidard, A., 2007. Historical reconstruction of the Atlantic Meridional Overturning Circulation from the ECMWF operational ocean reanalysis. Geophys. Res. Lett. 34.

Becker, J.J., Sandwell, D.T., Smith, W.H.F., Braud, J., Binder, B., Depner, J., Fabre, D., Factor, J., Ingalls, S., Kim, S.H., 2009. Global bathymetry and elevation data at 30 arc seconds resolution: SRTM30_plus. Mar. Geod. 32, 355–371.

Bell, M.J., Schiller, A., Le Traon, P.Y., Smith, N.R., Dombrowsky, E., Wilmer-Becker, K., 2015. An Introduction to GODAE OceanView. Taylor & Francis.

Boutin, J., Martin, N., Reverdin, G., Yin, X., Gaillard, F., 2013. Sea surface freshening inferred from SMOS and ARGO salinity: impact of rain. Ocean Sci. 9, 183.

Brasseur, P., Verron, J., 2006. The SEEK filter method for data assimilation in oceanography: a synthesis. Ocean Dyn. 56, 650–661.

Brodeau, L., 2007. Contribution à l'amélioration de la fonction de forçage des modèles de circulation générale océanique. Université Joseph-Fourier-Grenoble I Ph.D. thesis.

Brown, J.R., Power, S.B., Delage, F.P., Colman, R.A., Moise, A.F., Murphy, B.F., 2011. Evaluation of the South Pacific Convergence Zone in IPCC AR4 climate model simulations of the twentieth century. J. Clim. 24, 1565–1582.

Cabanes, C., Grouazel, A., von Schuckmann, K., Hamon, M., Turpin, V., Coatanoan, C., Paris, F., Guinehut, S., Boone, C., Ferry, N., de Boyer Montégut, C., Carval, T., Reverdin, G., Pouliquen, S., Le Traon, P.Y., 2013. The CORA dataset: validation and diagnostics of in-situ ocean temperature and salinity measurements. Ocean Sci. 9, 1–18. http://dx.doi.org/10.5194/os-9-1-2013.

Chambers, D.P., Cazenave, A., Champollion, N., Dieng, H., Llovel, W., Forsberg, R., von Schuckmann, K., Wada, Y., 2016. Evaluation of the global mean sea level budget between 1993 and 2014. Surv. Geophys. 38, 309–327.

Crosnier, L., Le Provost, C., 2007. Inter-comparing five forecast operational systems in the North Atlantic and Mediterranean basins: the MERSEA-strand1 Methodology. J. Mar. Syst. 65, 354–375.

Cunningham, S.A., Kanzow, T., Rayner, D., Baringer, M.O., Johns, W.E., Marotzke, J., Longworth, H.R., Grant, E.M., Hirschi, J.J.M., Beal, L.M., 2007. Temporal variability of the Atlantic meridional overturning circulation at 26.5 N. Science 317, 935–938.

Dee, D.P., Uppala, S.M., Simmons, A.J., Berrisford, P., Poli, P., Kobayashi, S., Andrae, U., Balmaseda, M.A., Balsamo, G., Bauer, P., Bechtold, P., Beljaars, A.C.M., van de Berg, L., Bidlot, J., Bormann, N., Delsol, C., Dragani, R., Fuentes, M., Geer, A.J., Haimberger, L., Healy, S.B., Hersbach, H., Hólm, E.V., Isaksen, L., Kållberg, P., Köhler, M., Matricardi, M., McNally, A.P., Monge-Sanz, B.M., Morcrette, J.J., Park, B.K., Peubey, C., de Rosnay, P., Tavolato, C., Thépaut, J.N., Vitart, F., 2011. The ERA-Interim reanalysis: configuration and performance of the data assimilation system. Q. J. R. Meteorol. Soc. 137, 553–597. http://dx.doi.org/10.1002/qj.828.

Desbruyères, D.G., Purkey, S.G., McDonagh, E.L., Johnson, G.C., King, B.A., 2016. Deep and abyssal ocean warming from 35 years of repeat hydrography. Geophys. Res. Lett. 43.

Desroziers, G., Berre, L., Chapnik, B., Poli, P., 2005. Diagnosis of observation, background and analysis-error statistics in observation space. Q. J. R. Meteorol. Soc. 131, 3385–3396.

Donguy, J.R., Meyers, G., 1996. Seasonal variation of sea-surface salinity and temperature in the tropical Indian Ocean. 43http://dx.doi.org/10.1016/0967-0637(96)00009-X.

Donlon, C.J., Martin, M., Stark, J., Roberts-Jones, J., Fiedler, E., Wimmer, W., 2012. The Operational Sea Surface Temperature and Sea Ice Analysis (OSTIA) system. Remote Sens. Environ. 116, 140–158. http://dx.doi.org/10.1016/j.rse.2010.10.017.

Drecourt, J.P., Haines, K., Martin, M., 2006. Influence of systematic error correction on the temporal behavior of an ocean model. J. Geophys. Res. Oceans 111.

Foltz, G.R., McPhaden, M.J., 2009. Impact of barrier layer thickness on SST in the central tropical North Atlantic. J. Clim. 22, 285–299.

Gasparin, F., Roemmich, D., 2016. The strong freshwater anomaly during the onset of the 2015/2016 El Nino. Geophys. Res. Lett. 43, 6452–6460. http://dx.doi.org/10.1002/2016GL069542.

Gasparin, F., Roemmich, D., 2017. The seasonal march of the equatorial Pacific upper-ocean and its El Niño variability. Prog. Oceanogr.

Good, S.A., Martin, M.J., Rayner, N.A., 2013. EN4: quality controlled ocean temperature and salinity profiles and monthly objective analyses with uncertainty estimates. J. Geophys. Res. Oceans 118, 6704–6716.

Haines, K., Johannessen, J., Knudsen, P., Lea, D., Rio, M.H., Bertino, L., Davidson, F., Hernandez, F., 2011. An ocean modelling and assimilation guide to using GOCE geoid products. Ocean Sci. 7, 151–164. http://dx.doi.org/10.5194/os-7-151-2011.

Hasson, A., Puy, M., Boutin, J., Guilyardi, E., Morrow, R., 2018. Northward pathway across the tropical north Pacific Ocean revealed by surface salinity: how do El Niño anomalies reach Hawaii? J. Geophys. Res. Oceans.

Hernandez, F., Blockley, E., Brassington, G.B., Davidson, F., Divakaran, P., Drévillon, M., Ishizaki, S., Garcia-Sotillo, M., Hogan, P.J., Lagemaa, P., Levier, B., Martin, M., Mehra, A., Mooers, C., Ferry, N., Ryan, A., Regnier, C., Sellar, A., Smith, G.C., Sofianos, S., Spindler, T., Volpe, G., Wilkin, J., Zaron, E.D., Zhang, A., 2015. Recent progress in performance evaluations and near real-time assessment of operational ocean products. J. Oper. Oceanogr. 8, s221–s238. http://dx.doi.org/10.1080/1755876X.2015.1050282.

Hu, S., Fedorov, A.V., 2016. Exceptionally strong easterly wind burst stalling El Niño of 2014. Proc. Natl. Acad. Sci. 113, 2005–2010.

Johnson, G.C., Lyman, J.M., Purkey, S.G., 2015. Informing deep Argo array design using Argo and full-depth hydrographic section data*. J. Atmos. Ocean. Technol. 32, 2187–2198.

Kelly, K.A., Small, R.J., Samelson, R.M., Qiu, B., Joyce, T.M., Kwon, Y.O., Cronin, M.F., 2010. Western boundary currents and frontal air–sea interaction: Gulf Stream and Kuroshio Extension. J. Clim. 23, 5644–5667.

Knight, J.R., Allan, R.J., Folland, C.K., Vellinga, M., Mann, M.E., 2005. A signature of persistent natural thermohaline circulation cycles in observed climate. Geophys. Res. Lett. 32.

Koenig, Z., Provost, C., Villacieros-Robineau, N., Sennéchael, N., Meyer, A., Lellouche, J.M., Garric, G., 2017. Atlantic waters inflow north of Svalbard: insights from IAOOS observations and Mercator Ocean global operational system during N-ICE2015. J. Geophys. Res. Oceans 122, 1254–1273.

Kolodziejczyk, N., Prigent-Mazella, A., Gaillard, F., 2017. ISAS-15 temperature and salinity gridded fields. SEANOEhttp://dx.doi.org/10.17882/52367.

Kouketsu, S., Kawano, T., Masuda, S., Sugiura, N., Sasaki, Y., Toyoda, T., Igarashi, H., Kawai, Y., Katsumata, K., Uchida, H., 2011. Deep ocean heat content changes estimated from observation and reanalysis product and their influence on sea level change. J. Geophys. Res. Oceans 116.

Labat, D., Ronchail, J., Guyot, J.L., 2005. Recent advances in wavelet analyses: part 2—Amazon, Parana, Orinoco and Congo discharges time scale variability. J. Hydrol. 314, 289–311.

Laurindo, L.C., Mariano, A.J., Lumpkin, R., 2017. An improved near-surface velocity climatology for the global ocean from drifter observations. Deep-Sea Res. I Oceanogr. Res. Pap. 124, 73–92. http://dx.doi.org/10.1016/j.dsr.2017.04.009.

Le Traon, P.Y., 2013. From satellite altimetry to Argo and operational oceanography: three revolutions in oceanography. Ocean Sci. 9, 901.

Lea, D.J., Drecourt, J.P., Haines, K., Martin, M.J., 2008. Ocean altimeter assimilation with observational-and model-bias correction. Q. J. R. Meteorol. Soc. 134, 1761–1774.

Lea, D.J., Martin, M.J., Oke, P.R., 2014. Demonstrating the complementarity of observations in an operational ocean forecasting system. Q. J. R. Meteorol. Soc. 140, 2037–2049.

Legler, D.M., Freeland, H.J., Lumpkin, R., Ball, G., McPhaden, M.J., North, S., Crowley, R., Goni, G.J., Send, U., Merrifield, M.A., 2015. The current status of the real-time in

situ global ocean observing system for operational oceanography. J. Oper. Oceanogr. 8, s189–s200.
Lellouche, J.M., Greiner, E., Le Galloudec, O., Garric, G., Regnier, C., Drevillon, M., Benkiran, M., Testut, C.E., Bourdalle-Badie, R., Gasparin, F., Hernandez, O., Levier, B., Drillet, Y., Remy, E., Le Traon, P.Y., 2018. Recent updates on the Copernicus Marine Service global ocean monitoring and forecasting real-time 1/12 high resolution system. Ocean Sci. Discuss. 2018, 1–70. http://dx.doi.org/10.5194/os-2018-15.
Lellouche, J.M., Le Galloudec, O., Drévillon, M., Régnier, C., Greiner, E., Garric, G., Ferry, N., Desportes, C., Testut, C.E., Bricaud, C., 2013. Evaluation of global monitoring and forecasting systems at Mercator Océan. Ocean Sci. 9, 57.
Levitus, S., 2005. Linear trends of zonally averaged thermosteric, halosteric, and total steric sea level for individual ocean basins and the world ocean, (1955–1959)–(1994–1998). Geophys. Res. Lett. 32. http://dx.doi.org/10.1029/2005GL023761.
Llovel, W., Lee, T., 2015. Importance and origin of halosteric contribution to sea level change in the southeast Indian Ocean during 2005–2013. Geophys. Res. Lett. 42http://dx.doi.org/10.1002/2014GL062611. 2014GL062611.
Madec, G., the NEMO team, 2008. Nemo ocean engine: note du pole de modélisation. In: Tech. Rep. Institut Pierre-Simon Laplace (IPSL), France, pp. 1288–1619 No 27 ISSN No.
Maes, C., McPhaden, M.J., Behringer, D., 2002. Signatures of salinity variability in tropical Pacific Ocean dynamic height anomalies. J. Geophys. Res. Oceans 107, 8012. http://dx.doi.org/10.1029/2000JC000737.
Purkey, S.G., Johnson, G.C., 2010. Warming of global abyssal and deep Southern Ocean waters between the 1990s and 2000s: contributions to global heat and sea level rise budgets*. J. Clim. 23, 6336–6351.
Raghukumar, K., Edwards, C.A., Goebel, N.L., Broquet, G., Veneziani, M., Moore, A.M., Zehr, J.P., 2015. Impact of assimilating physical oceanographic data on modeled ecosystem dynamics in the California Current System. Prog. Oceanogr. 138, 546–558.
Rao, R.R., Sivakumar, R., 2003. Seasonal variability of sea surface salinity and salt budget of the mixed layer of the north Indian Ocean. J. Geophys. Res. Oceans 108.
Reichler, T., Kim, J., 2008. How well do coupled models simulate today's climate? Bull. Am. Meteorol. Soc. 89, 303–311.
Reynolds, R.W., Rayner, N.A., Smith, T.M., Stokes, D.C., Wang, W., 2002. An improved in situ and satellite SST analysis for climate. J. Clim. 15, 1609–1625.
Rio, M.H., Mulet, S., Picot, N., 2014. Beyond GOCE for the ocean circulation estimate: synergetic use of altimetry, gravimetry, and in situ data provides new insight into geostrophic and Ekman currents. Geophys. Res. Lett. 41, 8918–8925.
Riser, S.C., Ren, L., Wong, A., 2008. Salinity in Argo: a modern view of a changing ocean. Oceanography 21, 56–67.
Roemmich, D., Church, J., Gilson, J., Monselesan, D., Sutton, P., Wijffels, S., 2015. Unabated planetary warming and its ocean structure since 2006. Nat. Clim. Chang. 5, 240–245. http://dx.doi.org/10.1038/nclimate2513.
Roemmich, D., Gilson, J., 2009. The 2004–2008 mean and annual cycle of temperature, salinity, and steric height in the global ocean from the Argo Program. Prog. Oceanogr. 82, 81–100.
Ryan, A., Regnier, C., Divakaran, P., Spindler, T., Mehra, A., Smith, G., Davidson, F., Hernandez, F., Maksymczuk, J., Liu, Y., 2015. GODAE OceanView Class 4 forecast verification framework: global ocean inter-comparison. J. Oper. Oceanogr. 8, s98–s111. http://dx.doi.org/10.1080/1755876X.2015.1022330.
She, J., Allen, I., Buch, E., Crise, A., Johannessen, J.A., Traon, P.Y.L., Lips, U., Nolan, G., Pinardi, N., Reissmann, J.H., 2016. Developing European operational oceanography for Blue Growth, climate change adaptation and mitigation, and ecosystem-based management. Ocean Sci. 12, 953–976.
Stepanov, V.N., Haines, K., Smith, G.C., 2012. Assimilation of RAPID array observations into an ocean model. Q. J. R. Meteorol. Soc. 138, 2105–2117. http://dx.doi.org/10.1002/qj.1945.
Stephens, G.L., L'Ecuyer, T., Forbes, R., Gettelmen, A., Golaz, J.C., Bodas-Salcedo, A., Suzuki, K., Gabriel, P., Haynes, J., 2010. Dreary state of precipitation in global models. J. Geophys. Res.-Atmos. 115, D24211. http://dx.doi.org/10.1029/2010JD014532.
Szekely, T., Gourrion, J., Pouliquen, S., Reverdin, G., 2016. CORA, Coriolis Ocean Dataset for Reanalysis. SEANOEhttp://dx.doi.org/10.17882/46219.
Tian, Y., Peters-Lidard, C.D., Eylander, J.B., Joyce, R.J., Huffman, G.J., Adler, R.F., Hsu, K.L., Turk, F.J., Garcia, M., Zeng, J., 2009. Component analysis of errors in satellite-based precipitation estimates. J. Geophys. Res.-Atmos. 114.
Toniazzo, T., Woolnough, S., 2014. Development of warm SST errors in the southern tropical Atlantic in CMIP5 decadal hindcasts. Clim. Dyn. 43, 2889–2913. http://dx.doi.org/10.1007/s00382-013-1691-2.
Vinogradova, N.T., Ponte, R.M., Fukumori, I., Wang, O., 2014. Estimating satellite salinity errors for assimilation of Aquarius and SMOS data into climate models. J. Geophys. Res. Oceans 119, 4732–4744.
Visbeck, M., Araujo, M., Boetius, A., Buch, E., Claustre, H., Dabrowski, T., Delory, E., de Young, B., Drinkwater, K., Fischer, A., others, 2015. More Integrated and More Sustainable Atlantic Ocean Observing (AtlantOS). In: CLIVAR Exchanges. 67. pp. 18–20.
Von Schuckmann, K., Le Traon, P.Y., 2011. How well can we derive Global Ocean Indicators from Argo data? Ocean Sci. 7, 783–791.
Von Schuckmann, K., Le Traon, P.Y., Alvarez-Fanjul, E., Axell, L., Balmaseda, M., Breivik, L.A., Brewin, R.J., Bricaud, C., Drevillon, M., Drillet, Y., 2016. The Copernicus marine environment monitoring service ocean state report. J. Oper. Oceanogr. 9, s235–s320.
Wang, G., Cheng, L., Boyer, T., Li, C., 2017. Halosteric sea level changes during the Argo era. Water 9, 484.
Wust, G., 1936. Oberflachensalzgehalt, Verdunstung und Niederschlag auf den Weltmeere, Landerkundliche Forschung, Festschrift f. Norbert Krebs.
Yin, X., Gruber, A., Arkin, P., 2004. Comparison of the GPCP and CMAP merged gauge–satellite monthly precipitation products for the period 1979–2001. J. Hydrometeorol. 5, 1207–1222.
Yu, L., 2011. A global relationship between the ocean water cycle and near-surface salinity. J. Geophys. Res. Oceans 116, C10025. http://dx.doi.org/10.1029/2010JC006937.